



# Parametric optimizing of electro-discharge machining for LM25Al/VC composite material machining using deterministic and stochastic methods

Mesay Alemu Tolcha<sup>1,2</sup> · Hirpa Gelgele Lemu<sup>2</sup>

Received: 23 November 2023 / Accepted: 6 February 2024  
© The Author(s) 2024

## Abstract

The electro-discharge machining (EDM) process is investigated using deterministic and stochastic methods to determine and model the effects of process parameters on machining performance. The workpiece utilized for the investigation was an LM25 aluminum alloy reinforced with vanadium carbide (VC), processed through a stir casting technique. EDM process parameters like peak current, discharge voltage, and pulse on-time are considered to analyze material removal rate, electrode wearing rate, and surface roughness. This study applied four multi-criteria decision-making (MCDM) and analytical methodologies to evaluate EDM performance. Then, the MCDM scores were compared using two objective verification mechanisms. In this case, the teaching-learning-based optimization (TLBO) technique delivered the best-desired results relative to the VIKOR, Grey relational grade (GRG), and the response surface method (RSM). Also, the RSM and analytical methods are simpler than the other methods, though they produced nearly identical results as the sophisticated MCDM and deterministic methods.

**Keywords** Multi-objective optimization · VIKOR · Vanadium carbide · Processing parameter · Analytical modeling · Material removal rate · Surface roughness

## 1 Introduction

The electro-discharge machining process (EDM) is a non-conventional and non-contact machining operation that is used in industry for high-precision products, especially in manufacturing industries, automotive industries, aerospace, communication, and biotechnology industries [1–3]. The majorities of those industries utilized materials with superior properties like high wear and corrosion resistance, low cost, low weight, and good strength to produce their products. In the same way, they are favored in some high-strength and high-temperature material applications. However, it is difficult to see the aforementioned properties in a single material,

and to cope with the obvious limitations of single materials, composite materials were proposed by different researchers [4–8]. Aluminum alloys are ideal engineering materials for different applications when supported by heat-refractory and hard materials. Vanadium carbide (VC) is a hard refractory material, and the cost of the reinforcement in comparison with other materials is very nominal [9, 10]. VC particulate reinforcements help to improve the aluminum matrix in terms of hardness, heat refraction, strength, and wear resistance [11]. In fact, extremely high hardness will lead to machinability challenges. When it comes to the machining of difficult-to-machine and/or hard materials, then selection and optimization of the appropriate machining techniques are of prime importance. In addition to their unique characteristics, most modern materials need special manufacturing processes to enable them to be machined with ease [12]. EDM, a thermo-physically based material ablation technology is a cutting-edge machining technique with a remarkable ability to machine extremely hard and brittle materials with complicated three-dimensional structures [13].

Studies show that the material removal rate decreased and the electrode wear increased with an increase in reinforcing quantity in the matrix phase [14, 15]. Some researchers

✉ Mesay Alemu Tolcha  
alemu170@yahoo.com

Hirpa Gelgele Lemu  
hirpa.g.lemu@uis.no

<sup>1</sup> Faculty of Mechanical Engineering, Jimma Institute of Technology, Jimma University, Jimma, Ethiopia

<sup>2</sup> Department of Mechanical and Structural Engineering, University of Stavanger, 4036 Stavanger, Norway

[16–19] have analyzed the feasibility of the composite materials in the EDM process and found that reinforcing constituents in the matrix obstruct effective sparking and reduce matrix phase erosion. To enhance the performance metrics of the EDM process, abundant sensitivity analysis and optimization of process variables with various high-strength and harder materials were also performed by different researchers [20–23]. According to different experimental findings, the results revealed that pulse current and discharge time significantly varied all the performance metrics (material removal rate and tool erosion rate) linearly with a gradual change [24, 25]. When milling NiTi alloy, Daneshmand et al. [26] focused on improving EDM process parameters to enhance the material removal rate. Voltage and current are the two most important elements influencing surface roughness [27]. Material removal rate rises with increasing current, surface roughness increases with increasing voltage and current, and white layer thickness grows with increasing voltage [28]. Most researchers [29–32] wanted to look into the effects of EDM parameters like discharge current and voltage, as well as the length of time between each off time and pulse on, relative electrode wear, the rate of material removal, and the surface roughness of different alloys.

In real applications, EDM process is complex, has time-varying characteristics, and stochastic [33]. The primary idea behind the EDM technique is to remove material from a workpiece using periodic electric discharges and thermo-electric power from an uncontacted electric electrode. To immerse the tool and workpiece, a pressured dielectric fluid is applied between the gap. Plasma channels emerge as a result of electron's avalanche motion and positive ions during spark generation. Ion collisions cause the formation of a high-temperature plasma channel [34]. Due to quick melting and evaporation, the material is removed from workpiece in the high-temperature zone [35]. Moreover, output results are drastically changed with process parameters such as workpiece properties (conductivities, ionization), machining settings (pulse on-time, pulse interval, flushing pressure, feed, etc.). The adaptation and control of process parameters to the machining situation depend on the analysis or identification of all these parameters. These variables can be analyzed by analytical and stochastic methods. The analytical method is a deterministic approach in which outcomes are determined through known relationships among state variables without room for random variation. However, the results provided by analytical models may or may not be accurate, depending on the assumptions that have been made in order to create the model. In many cases, it is difficult to model multiple variables at the same time using analytical models [36]. Stochastic analysis is one of the promising tools used for multi-criteria decision-making and then taking the necessary measures to improve existing deficiencies. On the other hand, stochastic analysis is a mathematical and statistical

representation of MCDM mode that allows random alternative solutions. In fact, stochastic multi-objective approaches also have difficulties achieving many goals at the same time [37–40]. Various approaches such as metaheuristics, Pareto-based strategies, teaching-learning-based optimization (TLBO), and multi-model independent direction are used to address the challenges.

Analytical modeling and MCDM analysis help decision makers for diversification or modification of the process parameters. Also, both models play a pivotal role in understanding process parameters and predict the performance of EDM with substantial quality machining of newcomer materials with greater flexibility to respond to demands of competitiveness and customer satisfaction. Rao et al. [41] employed a multi-objective TLBO algorithm with Grey relation grade (GRA) for EDM parametric optimization. Pratap et al. [42] also opted for the stochastic TLBO optimization technique to obtain the optimized process parameters for EDM EN31 machining. TLBO is a very frequently used technique in the multi-objective optimization. Likewise, optimization of the EDM process parameters by using VIKOR method during EDM process of titanium alloy was implemented by Manish and Pradhan [43]. VIKOR is a compromise solution for a problem with conflicting criteria that can help the decision makers to reach a final decision [44]. Karthikeyan et al. [45] and Kama et al. [46] used response surface methodology (RSM) and the VIKOR methods to obtain multi-objective optimization parameters for setting Al-SiC metal matrix composites (MMC) during EDM operation, and they suggested that these multi-objective optimization techniques are well suited to optimize the process parameters during any machining conditions. Optimization of process parameters in EDM process of Ti-6Al-4V alloy using hybrid Taguchi-based stochastic MOORA method was analyzed by Srikanth et al. [47]. It is widely used as a statistical approach for finding the best alternative solution from the various other alternatives available for the decision-making criteria. Tiwari et al. [48] attempted to find out the optimal combination of EDM process parameters using Taguchi fuzzy-based approach. Recently, uncertainties of input process parameters and heterogeneities of EDM process responses have been discussed in the literature from different perspectives [49–53]. The investigation of electro-discharge machining can nevertheless be broadly classified into two basic approaches: (1) analytical or stochastic approach, which includes experimental observation, and (2) theoretical calculations, ranging from electron physics to thermal conduction.

Furthermore, EDM process variables were optimized using different optimization techniques like Taguchi, the technique for order of preference by similarity to the ideal solution (TOPSIS), RSM, and GRA [54–59]. As a result, using various multi-standard methodologies may result in

varied choices. However, most of the approaches offered some unique advantages and also had deficiencies of one sort or another. On the other hand, the choice of those optimizer methods is based on the knowledge of researchers and professionals in the specific domain. In addition, the ML25Al/VC hybrid composite in the machining process is not yet fully understood due to the likely utilization of various materials for numerous non-convectional machining applications such as electrochemical machining, abrasive machining, and chemical machining. In addition, there is very little literature among the research done on the ML25Al/VC hybrid composite. Even it is possible to say that there are no works done on the ML25Al/VC under machining processes. While summarizing the advancements in using MCDM approaches, RSM, GRA, TLBO, and the VIKOR method are considered in this work with different weighting metrics for genuine factories and place options based on alternative ranking and instructional recorded in terms of quality from a multifaceted perspective.

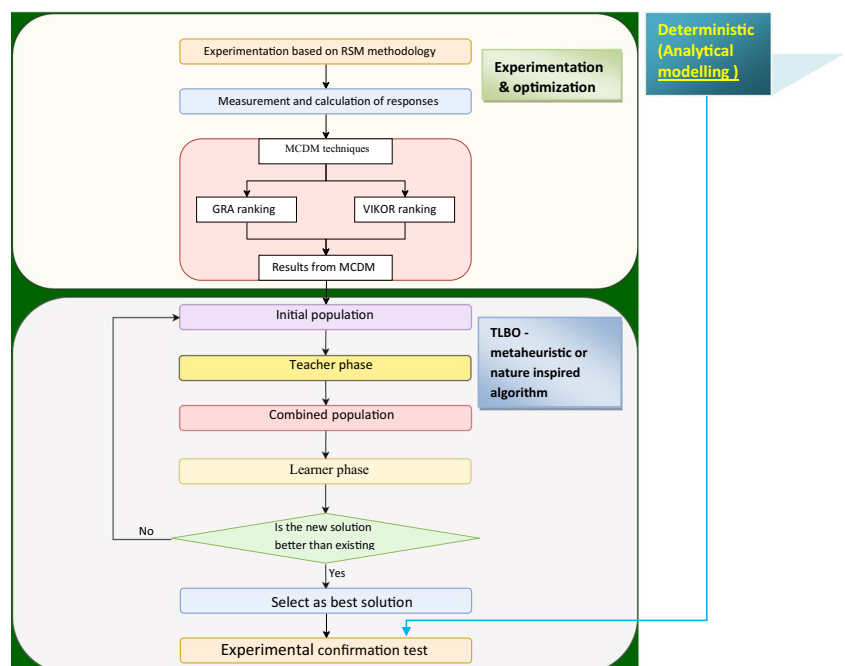
The main objective of this study is increasing the material removal rate (*MRR*), minimizing surface roughness ( $R_a$ ), and electrode wear rate (*EWR*) for composite aluminum alloys with vanadium carbide (LM25Al/VC) under EDM processes. The various EDM input parameters such as gap voltage, peak current, pulse on-time and pulse off-time, and VC weight percentage of reinforcement materials are considered in the analysis. Towards the end, the work focuses on deterministic and stochastic optimization, considering analytical modeling and MCDM optimization. The consistency and accuracy of the optimization capabilities depend on the quality of the assumptions made either during the definition

of the conditions or the solution process of the basic parametric relation with adequate information. To improve or accept the existing optimization methods, detailed analysis is important in a particular set of circumstances in order to properly describe the machinability of LM25Al/VC under the EDM process. This decision or selection should be based on a comparative evaluation of the model and its optimization capabilities. In addition to the dependence of the models on variations in the operation parameters, the initial assumptions should also be closely considered and understood. The work reported in this paper is organized as follows: Section 2 presents the methods and experimental design, considering base metal and reinforcement, analytical models, material removal, and product quality. Section 3 covers about multi-objective optimization, while Section 4 confirms the tests to validate the proposed models and optimization techniques based on considered parameters and the results obtained. The models and parametric relations describing input parameters and the performance of EDM are presented in Section 4.2. Finally, the conclusions drawn from the study are presented in Section 5.

## 2 Material and methods

In this work, analytical methods are considered before the generic form of experimental stochastic MCDM, VIKOR, and TLBO analysis. Analytical methods are fundamental to understanding the physics of the EDM process and its consequences. Figure 1 shows the procedure by which

Fig. 1 Conceptual outline of the research methods



the experimental work and electrical discharge machining parameter optimization are done.

### 2.1 Analytical modeling of material removal and product quality

In EDM process, the metal is removed from the workpiece and the tool electrode. *MRR* depends not only on the workpiece material but also on the tool electrode material and the machining variables such as electrode polarity, pulse conditions, machining medium, and plasma channel. Material removal mainly occurs due to intense localized heating almost by point heat source for a relatively short time. Such heating leads to melting and crater formation, as shown in Fig. 2.

The molten crater can be assumed to be hemispherical with a radius *r* which forms due to a single spark:

$$\vartheta = \frac{2}{3} \pi r^3 \tag{1}$$

Then, single-spark energy content in plasma channel can be given by

$$E_s = V_g I_p t_{on} \tag{2}$$

where *V<sub>g</sub>* is the voltage between the gap, *I<sub>p</sub>* is the peak current, and *t<sub>on</sub>* is the pulse on-time. In plasma channel

processing, spark energy gets lost due to dielectric medium heating, and the rest of the energy is distributed between the ions and impinging electrons [60]. Thus, the energy available to heat the workpiece is given by

$$E_w \propto E_s, E_w = H E_s \tag{3}$$

In the same way,

$$E_w \propto E_s \alpha \vartheta, \text{ then } \vartheta = G E_w = G V_g I_p t_{on} \tag{4}$$

where *H* and *G* are the material constants. Now *MRR* is the ratio of material removed in single-spark energy per cycle time and expressed as

$$MRR = \frac{\vartheta}{M_t} = \frac{G V_g I_p t_{on}}{t_{on} + t_{off}} \tag{5}$$

where *M<sub>t</sub>* is the machining time and *t<sub>off</sub>* is the pulse off-time. As indicated in Fig. 2, the radius of the hemispherical crater (*r*) is equal to height (*h*). Thus,

$$h \propto (\vartheta)^{1/3} \propto (V I_p t_{on})^{1/3}; \text{ then } h = K (V I_p t_{on})^{1/3} \tag{6}$$

The stochastic nature of the EDM process results in the random effect of discrete spark arcing and so on, which generates a rough surface and number of crater. On the other hand, the spark-machined surface consists of a multitude of overlapping craters that are formed by the action of microsecond duration

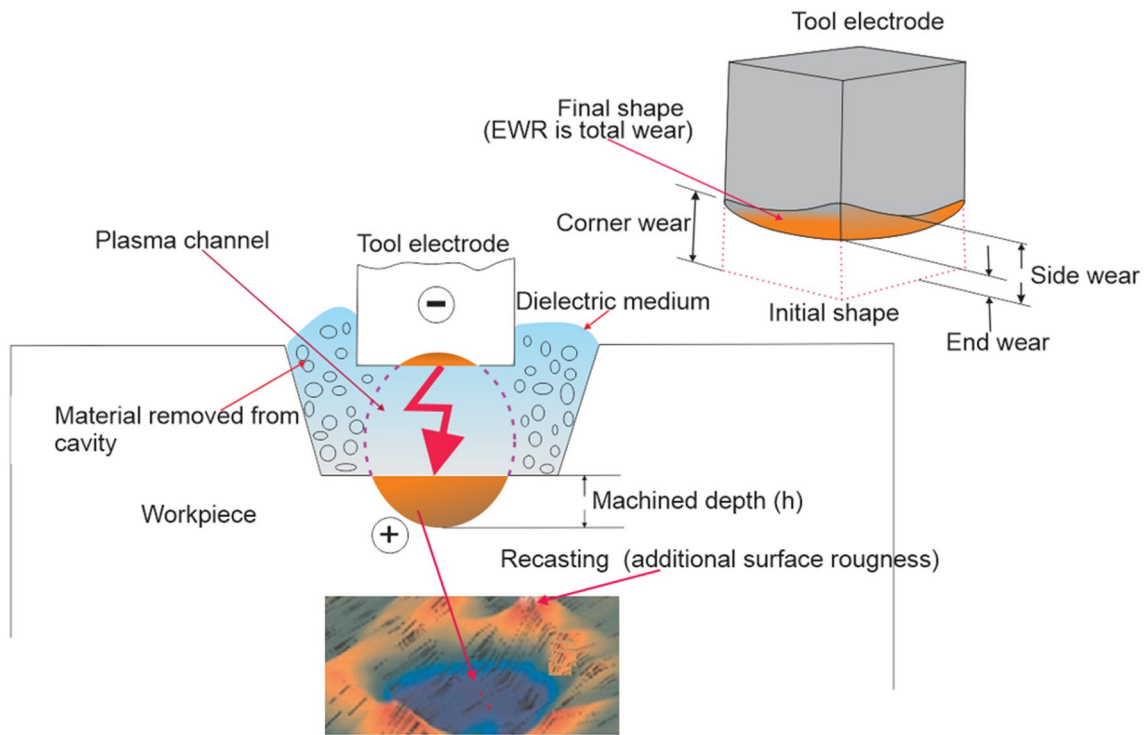


Fig. 2 Conceptual sketch of EDM process and product quality

spark discharges. Arithmetic mean surface roughness ( $R_a$ ) is type of surface parameter and used to describe an amplitude feature, which converts to roughness of the surface finish, which can be calculated using Eq. (7):

$$R_a = \frac{1}{L} \int |A| dx \tag{7}$$

where  $L$  is the sampling length of machined part,  $x$  is the profile direction, and  $A$  is the profile curve. In this work, the periodic profile and the arithmetic mean roughness is proposed with following relation:

$$R_a = \frac{h}{4} = \frac{K (V_g I_p t_{on})^{1/3}}{4} \tag{8}$$

With such high sparking frequencies, the combined effects of the individual sparks give substantial  $MRR$ . Likewise, sparking energy occurred randomly so that, over time, one gets a uniform average and total  $MRR$  over the whole workpiece cross section that can be calculated from

$$MRR_{total} = N_s \times \frac{GV_g I_p t_{on}}{t_{on} + t_{off}} \tag{9}$$

where  $k$  is the assumed material constant and  $N_s$  is the number of pulses per second. Further review was done to investigate the existing analytical models in the literature; no model has been found that is repeatable and gives better predictions than others at the level of mathematical models. After the preliminary investigation and tests, the exponential power function methods are proposed in this work for electrode wear ( $EWR$ ) and surface roughness. The investigation indicates that power functions have a better correlation with experimental results. The variables of  $a$ ,  $b$ , and  $c$  with EDM process parameters were formulated mathematically by using multi-objective power functions in the following forms:

$$R_a = M I_p^{a1} t_{on}^{b1} V_g^{c1} \tag{10}$$

$$EWR = N \frac{I_p^{a2} t_{on}^{b2} V_g^{c2}}{T_m} \tag{11}$$

$$T_r = Q \cdot \frac{EWR}{MRR} \tag{12}$$

where  $M$ ,  $N$ , and  $Q$  are assumed material constants and  $T_m$  ( $^{\circ}C$ ) is the melting point of the tool electrode (copper). Likewise,  $a1$ ,  $b1$ ,  $c1$ ,  $a2$ ,  $b2$ , and  $c2$  are constants. To obtain the values of assumed variables, python program was developed using curve fitting method corresponding to the experimental data. The estimated values and developed program are given in Appendix A.  $EWR$  depends on physical and mechanical properties, discharge energy, and pulse duration. The melting point is the most important factor in determining tool wear. Electrode wear in EDM has many forms, such as end wear, side wear, corner wear, and volume wear (Fig. 2). Electrode wear depends on a number of factors associated with the EDM, such as voltage, current, electrode material, and polarity [61].

### 2.2 Base metal and reinforcement

In this work, the LM25 Al alloy was considered the base material. To enhance the material characteristics of the LM25 Al alloy, vanadium carbide was used, whose chemical composition is shown in Table 1. Tests with VC often involve an oxide debasement. VC is produced by heating vanadium oxides with carbon to roughly  $1000^{\circ}C$  in a cupola furnace. Despite being thermodynamically stable, VC can be transformed to V2C at temperatures over  $1000^{\circ}C$ . VC particles are extremely strong at high temperatures and have a high oxidation capability [63]. As a result, it is used for a variety of high-temperature applications. The metal network composite used in this investigation was joined using a mix-projecting method. To combine the composite, a mix-projection arrangement comprised an obstruction stiffler heater and a hardened steel stirrer was used. The stirrer assembly consisted of a stirrer connected to a variable-speed vertical boring machine with a range of 80 to 1400 rpm through a steel shaft. The stirrer had three edges that were spaced by  $120^{\circ}$ . Within this approach, the liquid aluminum mixture (Al-LM25) was liquefied at a clear temperature near  $780^{\circ}C$  in the silent heater (furnace), and then a warmed support material with 3% wt of VC was blended with the liquid compound, and the mixture was mixed using the stirrer. The photographs of the fabricated composite samples are shown in Fig. 3. To achieve consistent composite characteristics, mixture composite was stirred at 800 rpm for 8 min. By controlling the stirring speed and cooling the casted material in the furnace by turning off the furnace, homogeneous of microstructure and mechanical properties can be improved. In addition, improvement depends on the amount and uniformity of

**Table 1** Chemical composition of base metals (LM25 AL and VC) [62]

Chemical composition	Cu	Mg	Si	Fe	Mn	Pb	Ni	Zn	Ti	Al
LM25 Al alloy	0.1	0.2–0.6	6.5–7.5	0.5	0.4	0	0.1	0.1	0.2	Bal.
VC	Cu	Cr	Si	Fe	C	Pb	O	N	Al	V
	0.003	0.006	0.005	0.005	0.01	0.001	0.025	0.006	0.005	Bal.



**Fig. 3** Photograph view of sample produced as workpiece at different speeds and temperatures

distribution of reinforcements, and the strength of the particle matrix boundary and the mechanical properties of the matrix. Subsequently, to investigate the effect of 3wt% VC in LM25 Al alloy, Brinell hardness as per ASTM E10 is  $363 \pm 16$  BNH obtained. When compared with the plain LM25 Al alloy, the hardness of synthesized composite increased up to 186%. This enhancement in hardness and strength value of LM25Al/VC are associated with the presence of VC as load bearing constituent in LM25 Al matrix during loading conditions. Similar phenomenon was reported in [63]. Table 2 shows the properties of the workpiece and electrode materials.

Before starting the machining of LM25Al/VC, energy-dispersive spectrometer (EDS) analysis was carried out to ensure the presence of reinforcement (VC) in the matrix phase, as shown in Fig. 4. It is observed from Fig. 4 that chemical constituents (Al, Si, Mn, Fe) of Al7075 were followed by the reinforcement elements such as V and C. This confirms the presence of VC particulates in LM25Al alloy matrix. ELEKTRA PLUS Spark EDM PS 50 ZNC series machine was used to conduct experimental work and the schematic diagram of EDM process, which is elucidated in Fig. 5, and machine specification are given in Table 3.

**Table 2** Thermal and mechanical properties of EDM electrode (copper) and material considered in this process (where data are collected from different literature and manuals)

Serial no.	Properties	Copper	Aluminum LM25	Vanadium carbide
1	Melting point, °C	1083	700	2730
2	Boiling point, °C	2580	3200*	3900
3	Thermal conductivity, W/m•K	398	150.62	168
4	Electrical conductivity, $A_g = 100$	97	39	--
5	Thermal expansion, per °C $\times 10^{-6}$	16	22	8
6	Compressive strength, MPa	45	120	607
7	Modulus of elasticity, GPa	124	71	420
8	Hardness, Rockwell A	35	55	91

An asterisk is considered in this table to indicate the evaporation of Al at 3200 C under the EDM process in which the properties deferment from the usual thermal properties of metals

**Fig. 4** EDS graph of LM25Al/VC before machining

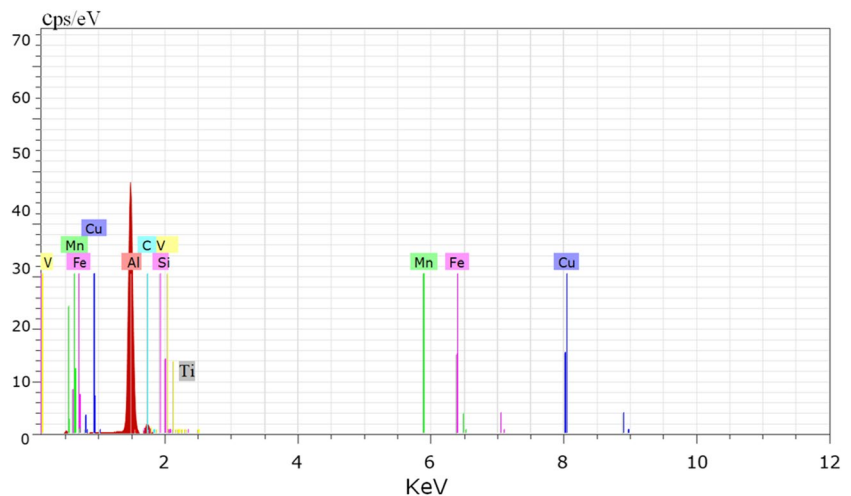


**Fig. 5** Schematic representation of EDM process

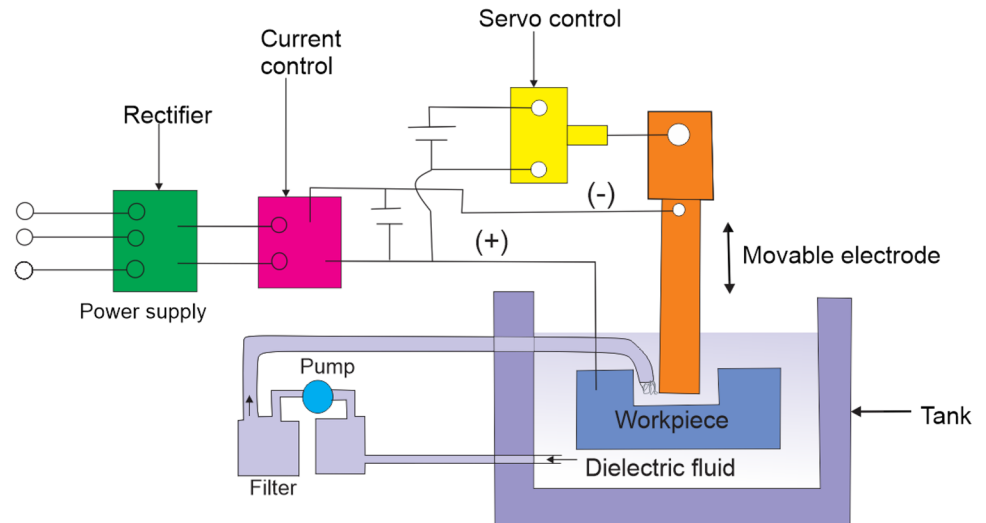


**Table 3** ELEKTRA PLUS Spark EDM PS 50 ZNC process parameter specifications

Parameters in EDM/EDM PS 50 ZNC	Specification range
Spark gap	10–125 $\mu\text{m}$
Spark frequency	200 to 500 kHz
Applied voltage	40 to 300 V
Peak voltage across the gap	30 to 250 V
Maximum material removal rate	0.6 g/min
Best surface finish*	0.8 $\mu\text{m}$
Pulse on-time	2 to 2400 $\mu\text{s}$
Peak current	0.5 to 70 A

\* To show the maximum surface finishing from the machine specification

In the same way, copper electrode and kerosene dielectric are used in this study. EDM process is influenced by both electrical and non-electrical parameters such as pulse on-time, flushing pressure, polarity, discharge current, electrode material, pulse interval, and open discharge voltage. It is difficult to examine the impact of all process parameters on performance characteristics at the same time due to different constraints. Thus, major influencing electrical parameters, namely, peak current  $I_p$ , voltage gap  $V_g$ , and pulse on-time  $t_{on}$ , were considered in this work. Because material removal rate is directly proportional to the amount of energy delivered, the peak current and the length of pulse on-time should be suitably managed [64, 65].

**Table 4** Experimental factors with five levels

Variables	Symbols	Units	Levels				
			1.682	-1	0	1	1.682
Peak current	$I_p$	A	5	6	8	10	11
Pulse on-time	$t_{on}$	$\mu\text{s}$	70	135	150	200	250
Voltage between the gap	$V_g$	V	45	50	60	70	75

### 2.3 Experimental design

The experiments were accomplished using three input parameters deferred at five levels, as shown in Table 4. The central composite design method of RSM is used in this research work to formulate the experimental trials using Minitab 21.2 software. Twenty runs were formulated by the Minitab software, and the number of trials purely depends on the number of process parameters and the five ranges selected in the experimental runs. The experimental runs comprised 8 factorial points ( $\pm 1$  level), 6 star points ( $\pm 1.68$  level), and 6 center points. Tests were carried out in a randomized way, and the weighted age of chosen EDM methodology variables on performance metrics, namely, material removal rate, tool electrode wear rate, and surface roughness, are considered responses. The independent inputs and their varying levels are delineated in Table 4. In the same way, fixed parameters are described in Table 5.

In addition, different combinations of process variables and their measured responses are delineated in Table 6. Analytical balance digital electronic A GN precision weight was used to measure the workpiece and electrode. The machinability of the processes is calculated by determining the material ablation rate, surface unevenness, and electrode erosion rate. The formulas used for measuring *MRR* and *EWR* are the following:

**Table 5** Fixed process parameters during machining process

Serial no.	Fixed parameters	Quantity
1	Working time	10 min
2	Flushing pressure	196 kPa
3	Anti-arc sensitivity	5
4	Servo sensitivity	6
5	Duty cycle	70%

$$MRR = \frac{W_{in} - W_{Fi}}{M_t} \left( \frac{g}{min} \right) \tag{13}$$

$$Electrode\ wear\ rate = \frac{W_{Ein} - W_{Efi}}{M_t} \left( \frac{g}{min} \right) \tag{14}$$

where  $w_{in}$  is the weight of the workpiece before machining,  $w_{fi}$  is the weight of the workpiece after machining,  $W_{Ein}$  is the weight of the electrode before machining, and  $W_{Efi}$  is the weight of the electrode after machining. The surface roughness is measured using Mitutoyo (SURFTEST SJ-210) surface roughness tester. It is important to state that when discharge current levels are less than 5 A, there is no much change in workpiece material ablation. In addition, higher levels of current greater than 15 A are not considered in order to facilitate stable machining and keeping parameter range consistence. To achieve the optimized parameter for

pulse on-time, a wide range has been chosen based on the machine capacity.

### 2.4 Regression modeling and checking its adequacy

Quadratic model suggested by fit summary method is utilized for prediction of  $MRR$ ,  $EWR$ , and  $R_a$ . The ANOVA test results of  $MRR$ ,  $EWR$ , and  $R_a$  are shown in Table 7. In ANOVA analyzing  $P_i$ -value helps to define the significance of the results in a statistical test. On the other hand, it shows the influence of the particular variable (factor) in terms of percentage on the response of the process. If  $P$ -value of the model is less than 0.05, then the model is ultimately specified as significant. Thus, the findings from ANOVA test on  $MRR$  data reveal that  $I_p$ ,  $t_{on}$ ,  $I_p^2$ ,  $t_{on}^2$ , and  $I_p \times t_{on}$  are essential variables to control  $MRR$  because their  $P$ -values fall below 0.05. The variables  $I_p$ ,  $t_{on}$ ,  $V_g$ ,  $I_p^2$ ,  $t_{on}^2$ ,  $V_g^2$ ,  $I_p \times t_{on}$ ,  $I_p \times V_g$ , and  $t_{on} \times V_g$  are the significant controllable parameters for  $EWR$ . Likewise,  $I_p$ ,  $t_{on}$ , and  $t_{on}^2$  are significant variables for  $R_a$ . The model  $F$ -values obtained for  $MRR$ ,  $EWR$ , and  $R_a$  are 32.77, 356.43, and 16.93, respectively. This  $F$ -ratio value shows that the formed performance models are outstanding since values greater than 0.05. Another possible way to confirm adequacy of the models is  $R$ -sq values and the evaluation represents the percentage of variation in a response variable that is explained by its relationship with predictor variables. In this case,  $R$ -sq values obtained for  $MRR$ ,  $EWR$ , and  $R_a$  are

**Table 6** Experimental trials and its responses

Experiment no.	Peak current, $I_p$ (A)	Pulse on-time, $t_{on}$ ( $\mu$ s)	Voltage, $V_g$ (V)	Material removal rate, $MRR$ (g/min)	Electrode wear rate, $EWR$ (g/min)	Surface roughness, $R_a$ ( $\mu$ m)
1	10	70	70	0.0295	0.0047	5.0572
2	8	135	60	0.0488	0.0060	4.0566
3	8	135	75	0.0540	0.0063	5.3428
4	6	70	50	0.0101	0.0013	7.1276
5	8	70	60	0.0106	0.0033	5.9171
6	10	200	50	0.0980	0.0086	3.7319
7	8	250	60	0.0694	0.0095	5.3777
8	10	70	50	0.0203	0.0048	4.9205
9	8	150	60	0.0651	0.0071	4.0487
10	6	200	50	0.0498	0.0063	4.8526
11	11	135	60	0.1085	0.0089	3.9106
12	5	135	60	0.0556	0.0053	5.2487
13	6	70	70	0.0191	0.0020	6.6376
14	6	200	70	0.0622	0.0090	6.3274
15	8	150	50	0.0594	0.0056	4.1176
16	8	135	45	0.0502	0.0045	4.7052
17	8	135	70	0.0587	0.0063	4.5427
18	10	200	70	0.0858	0.0097	4.0685
19	8	135	50	0.0533	0.0051	4.7225
20	8	135	70	0.0510	0.0067	4.1501



**Table 7** ANOVA table results for  $MRR$ ,  $EWR$ , and  $R_a$

Common variance	Source	DF	Analysis of variance for $MRR$				Analysis of variance for $EWR$				Analysis of variance for $R_a$			
			Adj SS	Adj MS	F-value	P-value	Adj SS	Adj MS	F-value	P-value	Adj SS	Adj MS	F-value	P-value
Model		9	0.0128	0.0014	32.77	0.000	0.0001	0.0000	356.43	0.000	13.705	1.523	16.93	0.000
Linear		3	0.0058	0.0019	44.45	0.000	0.0001	0.0000	681.19	0.000	4.600	1.533	17.05	0.000
	$I_p$	1	0.0027	0.0027	61.56	0.000	0.0000	0.0000	329.14	0.000	4.236	4.236	47.1	0.000
	$t_{on}$	1	0.0031	0.0031	71.66	0.000	0.0000	0.0000	1498.23	0.000	0.123	0.123	1.36	0.27
	$V_g$	1	0.0000	0.0000	0.18	0.677	0.0000	0.0000	227.99	0.000	0.238	0.238	2.64	0.135
Square		3	0.0029	0.0010	22.25	0.000	0.0000	0.0000	47.04	0.000	5.235	1.745	19.41	0.000
	$I_p \times I_p$	1	0.0009	0.0009	21.89	0.001	0.0000	0.0000	44.05	0.000	0.093	0.092	1.03	0.335
	$t_{on} \times t_{on}$	1	0.0019	0.0019	43.91	0.000	0.0000	0.0000	52.03	0.000	5.031	5.031	55.95	0.000
	$V_g \times V_g$	1	0.0001	0.0001	1.57	0.239	0.0000	0.0000	37.75	0.000	0.040	0.040	0.44	0.522
2-way interaction		3	0.0004	0.0001	3.42	0.061	0.0000	0.0000	31.7	0.000	0.264	0.088	0.98	0.441
	$I_p \times t_{on}$	1	0.0003	0.0003	7.57	0.02	0.0000	0.0000	37.71	0.000	0.025	0.024	0.27	0.613
	$I_p \times V_g$	1	0.0001	0.0001	1.7	0.221	0.0000	0.0000	20.06	0.001	0.010	0.010	0.11	0.751
	$t_{on} \times V_g$	1	0.0000	0.0000	0.99	0.342	0.0000	0.0000	37.33	0.000	0.230	0.230	2.56	0.141
Error		10	0.0004	0.0000			0.0000	0.0000			0.899	0.090		
	Lack-of-fit	8	0.0004	0.0000	1.52	0.562	0.0000	0.0000	0.51	0.803	0.873	0.097	3.74	0.382
	Pure error	2	0.0000	0.0000			0.0000	0.0000			0.026	0.026		
Total		19	0.0132				0.0001				14.605			
$R$ -sq														96.72%
$R$ -sq (adj)														99.69%
$R$ -sq (pred)														93.84%
														88.30%
														75.16%
														98.52%
														55.16

96.72%, 99.68%, and 93.84%, respectively. The lack-of-fit tests compare the residual error to the pure error from replicated design points. A lack-of-fit error significantly larger than the pure error for all responses indicates that non-significant of lack of fit is good. This obviously confirms that the developed second-order response models through RSM are sufficient and appropriate to predict the responses with minimized error. In general, the following equations characterize RSM's second-order surface interactions:

$$Response = a_0 + \sum_{n=i}^j a_n g_n + \sum_{n=i}^j a_{nn} g_n^2 + \sum_{n<m} a_{nm} g_n g_m + error \tag{15}$$

Thus,

$$MRR = -0.126 - 0.0304 I_p + 0.001157 t_{on} + 0.00544 V_g + 0.002485 I_p^2 - 0.000003 t_{on}^2 - 0.000030 V_g^2 + 0.000049 I_p \times t_{on} - 0.000152 I_p \times V_g - 0.000004 t_{on} \times V_g \tag{16}$$

$$EWR = -0.02284 + 0.000307 I_p + 0.000055 t_{on} + 0.000576 V_g + 0.000097 I_p^2 - 0.000000 t_{on}^2 - 0.000004 V_g^2 - 0.000003 I_p \times t_{on} - 0.000014 I_p \times V_g + 0.000001 t_{on} \times V_g \tag{17}$$

$$R_a = 16.99 - 0.680 I_p - 0.0752 t_{on} - 0.101 V_g + 0.0245 I_p^2 + 0.000170 t_{on}^2 + 0.00072 V_g^2 + 0.000426 I_p \times t_{on} - 0.00173 I_p \times V_g + 0.000260 t_{on} \times V_g \tag{18}$$

Figures 6, 7, and 8 show the interaction plots for  $MRR$ ,  $EWR$ , and  $R_a$ , respectively, as a function of the corresponding input variables. The results show that process parameters such as pulse on-time, peak current, and gap voltage influence the performance of the machine in different ways. Similarly, Figures 9, 10, and 11 show the predicted values for  $MRR$ ,  $EWR$ , and  $R_a$ , respectively, function of the corresponding actual values. All of the data lies along a straight line, indicating that the model is acceptable.

At the end, corresponding to the number of experimental runs 3D profiles of  $MRR$ ,  $EWR$ , and  $R_a$  were computed and shown in Fig. 12. The results show that random process parameter input for EDM can generate random performance output.

### 3 Multi-objective optimization

Surface response method experimental philosophy is focused on optimizing the process parameters in the perspective of a single quality criterion which does not give

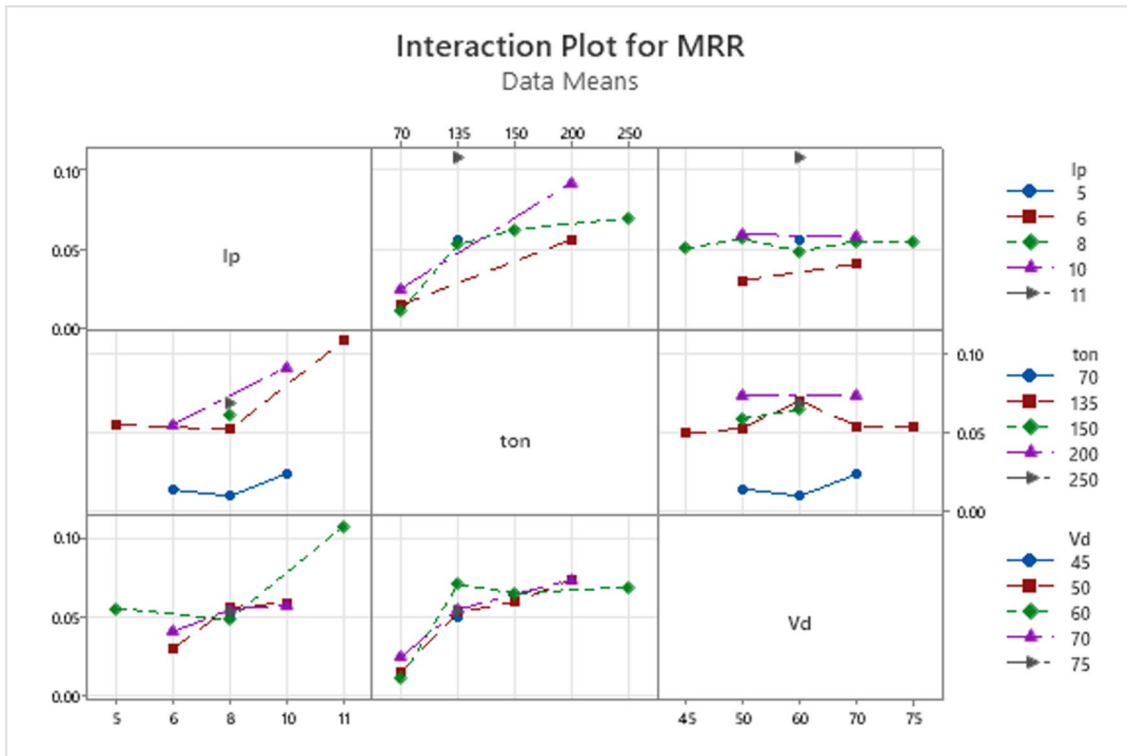


Fig. 6 Interaction and effect of input variables  $I_p$ ,  $t_{on}$ , and  $V_g$  values on  $MRR$  results

sufficient idea about the influence on other performance characteristic involvement [66]. Surface response methods cannot solve a multi-response optimization problem.

On other the hand, RM technique is often combined with multi-objective optimization techniques to switch a multi-decision making technique to a single-objective

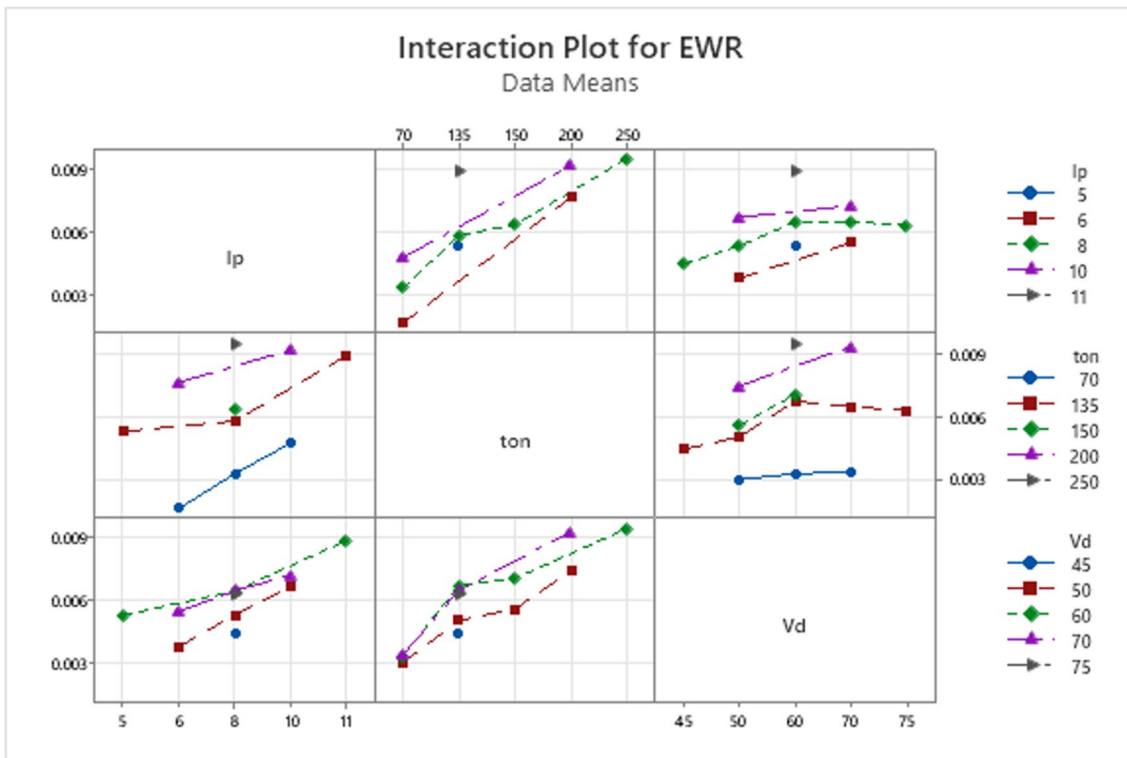


Fig. 7 Interaction and effect of input variables  $I_p$ ,  $t_{on}$ , and  $V_g$  values on  $EWR$  results

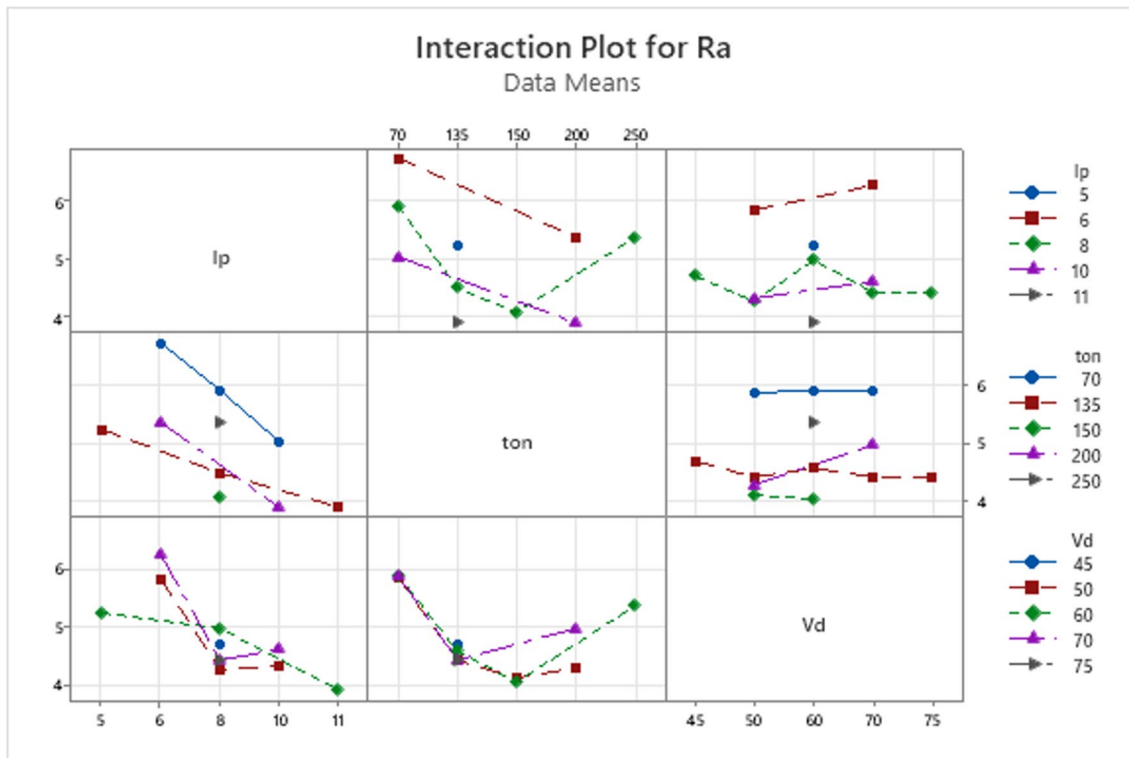
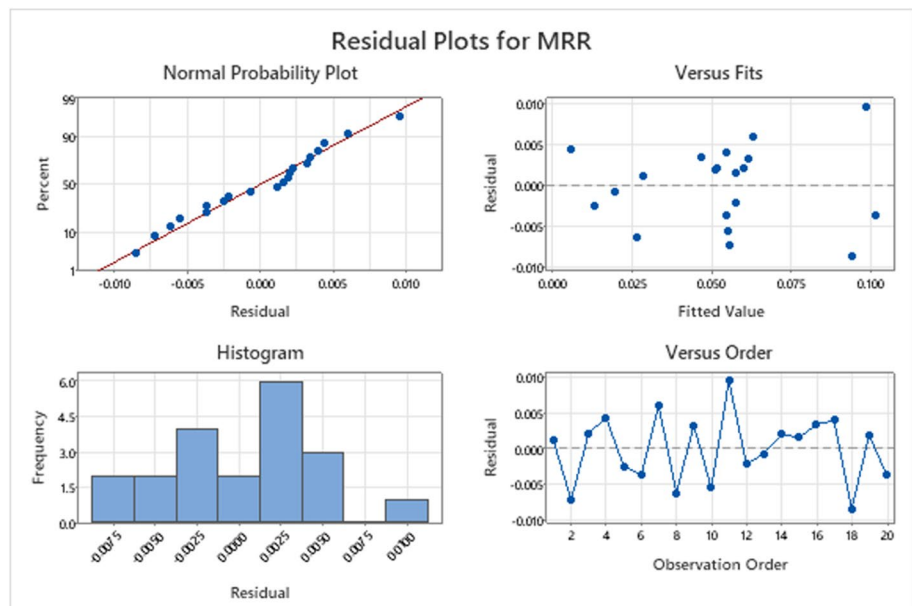


Fig. 8 Interaction and effect of input variables  $I_p$ ,  $t_{on}$ , and  $V_g$  values on  $R_a$  results

Fig. 9 Material removal rate residual diagrams



optimization problem. Hence, multi-objective optimization techniques are implemented where the quality characteristics are optimized and the results for the best levels are obtained. In this work, Grey relational grade (GRG) and VKOR are considered to resolve problems using complex inter-relationships among the multiple performance

characteristics. In fact, Grey relational grade technique provides an approach to create an idea about the system which is indecisive, incomplete, and not apparent. The procedure of GRG includes the consideration of different output parameters that may have different characteristics. Thus, by performing GRG on such problems, the

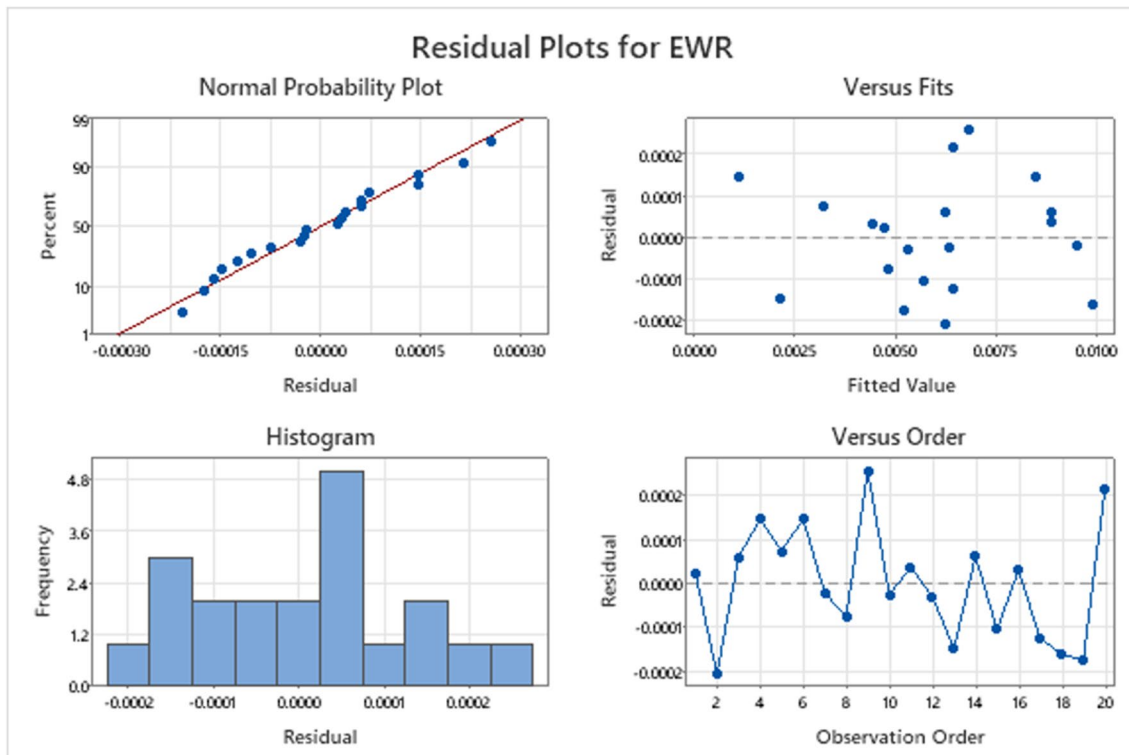


Fig. 10 Electrode wear rate residual diagrams

multi-objective is converted into a single objective as given in Table 8. Steps involved in GRA are the following:

Step 1: Normalization of the performance measures from 0 to 1.

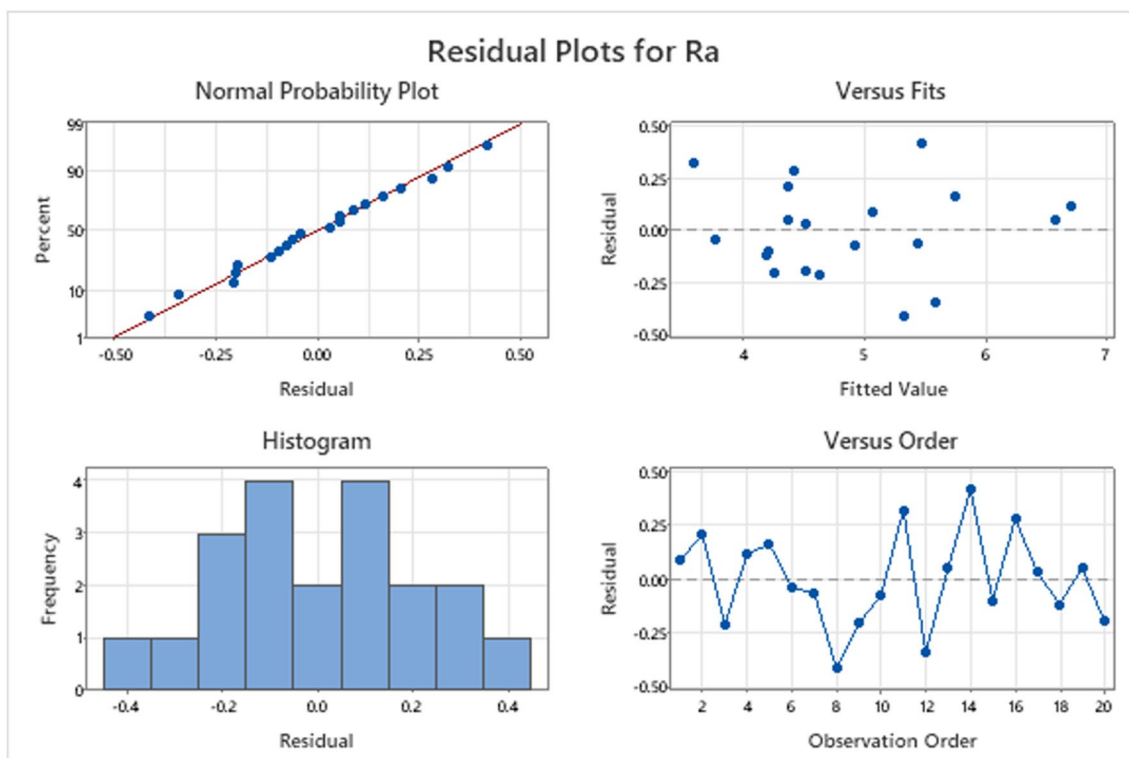
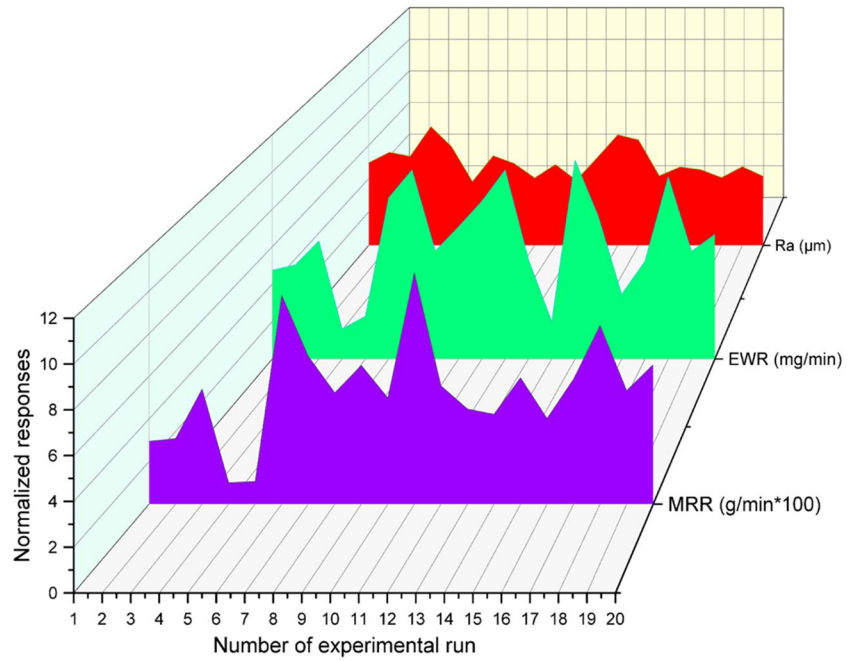


Fig. 11 Surface roughness residual diagram

**Fig. 12** The 3D responses profile (*MRR*, *EWR*, and *R<sub>a</sub>*) versus number of experiment run



Step 2: The Grey relational coefficient (GRC) establishes the correlation between the normalized experimental response that is desired and the actual response. The value of GRC is calculated using the relation provided in Eq. 19.

$$\varphi_i(G) = \frac{\Delta_{min} + \varphi\Delta_{max}}{\Delta_{oi}(G) + \varphi\Delta_{max}} \quad (19)$$

where,  $\Delta(G)$  is the deviation sequence, *i.e.*,  $\Delta_{oi}(G) = |g_i(G) - x_i(G)|$ ;  $\varphi$  is the unique coefficient which sustains between 0 and 1 (usually assumed as  $\varphi = 0.5$ ); (*G*) is a GRC;  $\Delta_{min}$  (least deviation sequence) is the lowest value of  $\Delta_{oi}(G)$ ; and  $\Delta_{max}$  (highest deviation sequence) is the highest value of  $\Delta_{oi}(G)$ .

Step 3: Grey relational grade is found out by averaging the Grey relational coefficient values; best value of GRG is obtained in experiment run 11 and the optimal combination of peak current 11 A, pulse on-time 135  $\mu$ s, and gap voltage 60 V. For further optimization, GRG is considered an output response, and RSM parametric optimization is done on GRG. For a better maximization characteristic, the predicted input parameters are peak current of 11 A, pulse time of 175  $\mu$ s, and gap voltage of 45 V, which maximize *MRR* and minimize *EWR* and *R<sub>a</sub>*.

### 3.1 VIKOR

VIKOR means multi-criterion optimization and comprising solution. The VIKOR technique focuses on positioning and picking an ideal substitute from a set of options and gives compromise answer for an issue with clashing measures and hence coming to a last arrangement. It is a powerful

apparatus for the advancement of machining activity which comprises different reactions [67]. The proposed technique contains the following steps:

*Step 1:* Development of selection framework that comprises all the data about the traits and the options of the interaction. Here, the potential options are addressed in line ( $i = 1, 2...m$ ) and all credits connecting with every one of the choices are portrayed in the section ( $j = 1, 2... n$ ).

*Step 2:* Get the normalization choice framework utilizing the formulae given underneath, where  $x_{ij}$  is the standardize choice. The normalized decision matrix grid can be addressed.

$$\bar{X}_{ij} = \frac{x_{ij}}{\sqrt{\sum_{i=1}^n (X_{ij})^2}} \quad (20)$$

*Step 3:* Acquire the weighted standardized choice network by assigning the heaviness of each property as  $\{w_j, j = 1, 2...n\}$ . It may be very well resolved utilizing the formulae given underneath (Eq. (21)):

$$W_{ij} = w_j \times \bar{X}_{ij} \quad (21)$$

where  $w_j$  is assigned a value as weight for responses and the sum of assigned values should be equal to 1. Thus, weights of 0.35 are assigned to *MRR* and *EWR*, and weight 0.3 is assigned to *R<sub>a</sub>*.

*Step 4:* Standardize the choice lattice amounts somewhere in the range of 0 and 1. The information standardization is done utilizing the accompanying condition. The normalized choice grid can be composed as formulated in Eqs. (22) and (23):

**Table 8** Grey relational analysis from experiment results (as initial random population for TLBO also)

Experimental run	Normalization			Deviation sequence			Grey relational coefficient (GRC)			Grade analysis grade	
	<i>MRR</i>	<i>EWR</i>	<i>R<sub>a</sub></i>	<i>MRR</i>	<i>EWR</i>	<i>R<sub>a</sub></i>	<i>MRR</i>	<i>EWR</i>	<i>R<sub>a</sub></i>	GRG	Rank
1	0.1974	0.5910	0.6097	0.8026	0.4090	0.3903	0.3838	0.5501	0.5616	0.4985	15
2	0.3929	0.4385	0.9044	0.6071	0.5615	0.0956	0.4516	0.4710	0.8395	0.5874	6
3	0.4462	0.4054	0.5256	0.5538	0.5946	0.4744	0.4745	0.4568	0.5131	0.4815	18
4	0.0000	1.0000	0.0000	1.0000	0.0000	1.0000	0.3333	1.0000	0.3333	0.5556	8
5	0.0057	0.7613	0.3565	0.9943	0.2387	0.6435	0.3346	0.6769	0.4373	0.4829	17
6	0.8931	0.1324	1.0000	0.1069	0.8676	0.0000	0.8239	0.3656	1.0000	0.7298	2
7	0.6024	0.0282	0.5153	0.3976	0.9718	0.4847	0.5571	0.3397	0.5078	0.4682	19
8	0.1034	0.5875	0.6500	0.8966	0.4125	0.3500	0.3580	0.5479	0.5882	0.4981	16
9	0.5593	0.3156	0.9067	0.4407	0.6844	0.0933	0.5315	0.4222	0.8427	0.5988	5
10	0.4039	0.4061	0.6700	0.5961	0.5939	0.3300	0.4561	0.4571	0.6024	0.5052	14
11	<b>1.0000</b>	0.0981	<b>0.9474</b>	<b>0.0000</b>	<b>0.9019</b>	<b>0.0526</b>	<b>1.0000</b>	<b>0.3567</b>	<b>0.9047</b>	<b>0.7538</b>	<b>1</b>
12	0.4622	0.5236	0.5533	0.5378	0.4764	0.4467	0.4818	0.5121	0.5282	0.5073	13
13	0.0917	0.9149	0.1443	0.9083	0.0851	0.8557	0.3550	0.8545	0.3688	0.5261	12
14	0.5291	0.0922	0.2357	0.4709	0.9078	0.7643	0.5150	0.3552	0.3955	0.4219	20
15	0.5006	0.4884	0.8864	0.4994	0.5116	0.1136	0.5003	0.4943	0.8149	0.6031	4
16	0.4075	0.6253	0.7134	0.5925	0.3747	0.2866	0.4577	0.5716	0.6356	0.5550	9
17	0.4939	0.4043	0.7612	0.5061	0.5957	0.2388	0.4969	0.4563	0.6768	0.5434	11
18	0.7693	0.0000	0.9009	0.2307	1.0000	0.0991	0.6843	0.3333	0.8346	<b>0.6174</b>	3
19	0.4388	0.5544	0.7083	0.5612	0.4456	0.2917	0.4712	0.5288	0.6315	0.5438	10
20	0.4158	0.3641	0.8768	0.5842	0.6359	0.1232	0.4612	0.4402	0.8024	0.5679	7

**Table 9** Optimization of parameters utilizing VIKOR optimization technique

Experimental run	Normalized decision mat			Weight standardization			Standardized ideal		VIKOR file	
	<i>MRR</i>	<i>EWR</i>	<i>R<sub>a</sub></i>	<i>MRR</i>	<i>EWR</i>	<i>R<sub>a</sub></i>	<i>Y<sub>i</sub></i>	<i>R<sub>i</sub></i>	<i>Q<sub>i</sub></i>	Rank
1	0.1121	0.1639	0.2325	0.2809	0.1431	0.1381	0.5622	0.2809	0.6172	13
2	0.1852	0.2086	0.2063	0.2125	0.1965	0.0818	0.4908	0.2125	0.3176	4
3	0.2051	0.2182	0.1996	0.1938	0.2081	0.0674	0.4693	0.2081	0.2749	10
4	0.0382	0.0443	0.3079	0.3500	0.0000	0.3000	0.6500	0.3500	0.9416	19
5	0.0404	0.1141	0.2668	0.3480	0.0835	0.2118	0.6433	0.3480	0.9264	20
6	0.3722	0.2981	0.1683	0.0374	0.3037	0.0000	0.3411	0.3037	0.3757	11
7	0.2635	0.3286	0.2425	0.1391	0.3401	0.1595	0.6388	0.3401	0.8970	17
8	0.0769	0.1650	0.2219	0.3138	0.1444	0.1152	0.5734	0.3138	0.7290	15
9	0.2474	0.2445	0.1826	0.1543	0.2395	0.0307	0.4245	0.2395	0.3044	6
10	0.1893	0.2180	0.2188	0.2086	0.2078	0.1086	0.5251	0.2086	0.3542	10
11	0.4122	0.3082	0.1763	0.0000	0.3157	0.0173	0.3330	0.3157	0.3996	12
12	0.2111	0.1836	0.2367	0.1882	0.1667	0.1470	0.5020	0.1882	0.2622	3
13	0.0725	0.0692	0.2993	0.3179	0.0298	0.2816	0.6293	0.3179	0.8188	16
14	0.2361	0.3099	0.2657	0.1648	0.3177	0.2094	0.6919	0.3177	0.9056	18
15	0.2254	0.1940	0.1857	0.1748	0.1791	0.0374	0.3912	0.1791	0.0811	9
16	0.1906	0.1539	0.2122	0.2074	0.1311	0.0943	0.4328	0.2074	0.2219	2
17	0.2229	0.2186	0.2048	0.1772	0.2085	0.0786	0.4642	0.2085	0.2690	5
18	0.3259	0.3369	0.1835	0.0807	0.3500	0.0326	0.4634	0.3500	0.6816	14
19	<b>0.2023</b>	<b>0.1747</b>	<b>0.1994</b>	<b>0.1964</b>	<b>0.1560</b>	<b>0.0669</b>	<b>0.4193</b>	<b>0.1964</b>	<b>0.1710</b>	<b>1</b>
20	0.1938	0.2303	0.1946	0.2045	0.2226	0.0565	0.4835	0.2226	0.3370	8

$$Y_i^+ = \sum_{j=1}^n W_j \left[ \frac{(X_{ij})_{max} - (X_{ij})}{(X_{ij})_{max} - (X_{ij})_{min}} \right], \quad (22)$$

for beneficial attribute

$$Y_i^- = \sum_{j=1}^n W_j \left[ \frac{(X_{ij}) - (X_{ij})_{min}}{(X_{ij})_{max} - (X_{ij})_{min}} \right], \quad (23)$$

non – beneficial attribute

Step 5: Register the gainful (ideal) and non-valuable (non-ideal) arrangements. These qualities can be determined utilizing the conditions indicated underneath:

$$R_i = \text{Max}^n \text{ of } \left\{ w_j \left[ \frac{(X_{ij})_{max} - (X_{ij})}{(X_{ij})_{max} - (X_{ij})_{min}} \right] \right\} \quad (24)$$

Step 6: Decide the utility measure and the lament measure by utilizing the accompanying conditions. Towards the end, the VIKOR file ( $Q_i$ ) is generated utilizing the condition given underneath (Eq. 11), where  $Q_i$  signifies the VIKOR file esteem  $i = 1, 2 \dots n$ ; likewise,  $v$  addresses the heaviness of the most extreme gathering utility (in this work,  $v$  is 0.5).

$$Q_i = \frac{v((Y_i - Y_{i-min}))}{((Y_{i-max} - Y_{i-min}))} + (1 - v) \left( \frac{((R_i - R_{i-min}))}{((R_{i-max} - R_{i-min}))} \right) \quad (25)$$

Here  $Y_{i-max}$  is the maximum value of  $Y_i$  and  $Y_{i-min}$  is the minimum value of  $Y_i$ ;  $R_{i-max}$  is the maximum value of  $R_i$ , and  $R_{i-min}$  is the minimum value of  $R_i$ .

Step 7: Ranking the acceptance choice with the cases:

- Case 1:  $Q(a2) - Q(a1) \geq 1/(n - 1)$  (depending on the objective faction preference) and
- Case 2: acceptance stability likewise  $Q_j$  is ranking by  $Y_i$  and or  $R_i$  with  $v \geq 0.5$  in light of VIKOR file  $Q_i$ .

The option with the biggest  $Q_i$  esteem is considered in this work as the best arrangement and result generated in Table 9.

The result obtained from VIKOR optimization technique and portrayed in Table 9 fulfilled the first case of acceptable advantage criteria from  $Q_i$  file. The optimal condition is analyzed using closeness to the ideal solution and rank; best value of VIOR is obtained in experiment run 19 and the optimal combination of peak current 8 A, pulse on-time 135  $\mu$ s, and gap voltage 50 V. In the same way, further minimization characteristics are applied using the RSM optimizer, and the predicted input parameters are obtained, like a peak current of 10 A, a pulse time of 168  $\mu$ s, and a gap voltage of 48 V for maximum  $MRR$ , and minimum  $EWR$  and  $R_a$ .

### 3.2 TLBO algorithm

Teaching learning-based optimization (TLBO) is population-based algorithm inspired by learning process in a class room between students and teacher [41, 68]. The output in TLBO algorithm is considered in term of results or grade of the learners which depends on the quality of teacher. The current work was centered on maximization of  $MRR$ , and minimization of  $EWR$  and  $R_a$ . The detailed steps of TLBO algorithm are delineated in Fig. 1. Additionally, the parametric bounds are delineated in the following equation:

Step 1: Parameter bounds

$$\text{Peak current} : 5 \leq I_p \leq 11 \quad (26)$$

$$\text{Pulse on – time} : 70 \leq t_{on} \leq 250 \quad (27)$$

$$\text{Gap voltage} : 45 \leq V_g \leq 75 \quad (28)$$

Step 2: Select the size of the population (number of experiments),  $N_p = 20$

Step 3: The teaching process can be formulated as follows:

$$X_{new\_ij} = X_{ij} + r_i (X_{best} - T_f \cdot X_{mean}) \quad (29)$$

where  $X_{ij}$  is the inputted parameter as learners’ subjects.  $X_{best}$  is the result of the best parameter (i.e., the teacher) in the GRG.  $T_f$  is the teaching factor which decides the value of mean to be changed and  $r_i$  is the random number in the range [0,1].  $T_f$  is not a parameter in this TLBO algorithm and its value can be either 1 or 2. The value of  $T_f$  is randomly decided as

$$T_f = \text{round} [1 + \text{rand}(0, 1)\{2 - 1\}] \quad (30)$$

Step 4: Calculate the new response and then apply greedy selection. At the end, accept  $X_{new\_ij}$  if it gives a better solution and  $X_{new\_ij}$  failed between bounded values; otherwise, repeat the step in Eq. (28).

Step 5: This phase of the algorithm simulates the process parameters as learners through mutual interaction among themselves. Students can also enhance their knowledge by discussing or interacting with other students. This learning phenomenon can be expressed as follows:

For maximization with greedy selection,

$$X_{new\_ij} = X_{ij} + r_i (X_{ij} - X_p) \text{ if Response } i > \text{Response } p \quad (31)$$

$$X_{new\_ij} = X_{ij} - r_i (X_{ij} - X_p) \text{ if Response } i < \text{Response } p \quad (32)$$

For minimization target,

$$X_{new\_ij} = X_{ij} - r_i(X_{ij} - X_p) \text{ if Response } i > \text{Response } p$$

$$X_{new\_ij} = X_{ij} + r_i(X_{ij} - X_p) \text{ if Response } i < \text{Response } p$$

(33)

(34)

```

import numpy as np
import random
def TLBO(Response_function, num_factors, lb,ub, num_ iterations, Run_size):
    Run=np.random.uniform(lb,ub, size=(Run_size, num_factors))
    Response=np.array([Response_function(individual) for individual in Run])
    # find the best solution (Grade analysis grade ranking)
    best_GRG=np.argmax(Response)
    best_solution=Run[best_GRG]
    best_Response=Response(best_GRG)
    #Iterate
    for i in range(num_ iterations):
        #Teaching phase
        mean_solution=np.mean(Run, axis=0)
        sorted_indices=np.argsort(Response)[::-1]
        #instead of sequence [START: STOP: STEP], [-1] and [0] are used
        # best teacher by factor is represented as as best individual in this program
        best_individual=Run[sorted_indices[0]]
        worst_individual=Run[sorted_indices[-1]]
        delt=best_individual- mean_solution
        New_boundedfactors=mean_solution +
np.random.normal(size=(Run_size,num_factors))*delt
        New_boundedfactors=np.clip(New_boundedfactors,lb,ub)
        New_Response=np.array([Response_function(individual) for individual in
New_boundedfactors])
        replace_indices=np.where(New_Response > Response)[0]
        Run[replace_indices]= New_boundedfactors[replace_indices]
        Response[replace_indices]= New_Response[replace_indices]
        #Learner phases
        for j in range(Run_size):
            r1=np.randint(Run_size)
            while r1==j:
                r1=np.random.randint(Run_size)
            r2=np.random.randint(Run_size)
            while r2==j or r2==r1:
                teacher=Run[sorted_indices[0]]
                if Response[r1] > Response[r2]:
                    learner=Run[r1]
                delt2=teacher-learner
                New_boundedfactorslearner= learner + np.random.normal()*delt2
                New_boundedfactorslearner=np.clip(New_boundedfactorslearner, lb,ub)
                New_Responselearner = Response_function(New_boundedfactorslearner)
                if New_Responselearner > Response[j]:
                    Run[j]= New_Responselearner
    # Return the solution found
    best_GRG=np.argmax(Response)
    best_solution=Run[best_GRG]
    best_Response=Response(best_GRG)
    return best_solution, best_Response

```



**Table 10** Teacher phase-updated process parameter and response

Run no.	Input parameters			Bounded input parameters			New responses			Grade analysis grade	
	$I_p$	$t_{on}$	$V_g$	$I_p$	$t_{on}$	$V_g$	$MRR$	$EWR$	$R_a$	GRG	Rank
1	10	70	70	9.48	70.00	59.86	0.0291	0.0070	5.2540	0.4939	15
2	8	135	60	6.79	119.73	49.84	0.0457	0.0079	5.0306	0.5145	8
3	8	135	75	5.09	134.98	49.78	0.0574	0.0085	5.5116	0.5556	7
4	6	70	50	10.80	200.00	51.00	0.1384	0.0178	3.6546	0.6528	2
5	8	70	60	8	158	53	0.0751	0.0125	4.1456	0.5145	8
6	10	200	50	7	125	63	0.0583	0.0104	4.8445	0.6528	2
7	8	250	60	10	224	48	0.1239	0.0180	4.1194	0.5145	8
8	10	70	50	7	208	66	0.0836	0.0190	5.0251	0.6528	2
9	8	150	60	8	143	73	0.0693	0.0133	4.5363	0.5145	8
10	6	200	50	7	172	54	0.0741	0.0133	4.4594	0.6528	2
11	11	135	60	6	178	57	0.0756	0.0143	4.8923	0.5145	8
12	5	135	60	9	156	70	0.0852	0.0150	4.0934	0.5145	8
13	6	70	70	8	173	59	0.0835	0.0148	4.1749	0.4939	15
14	6	200	70	10	193	58	0.1186	0.0178	3.7716	0.4939	15
15	8	140	60	8	77	45	0.0110	0.0045	5.8443	0.5145	8
16	<b>8</b>	<b>135</b>	<b>45</b>	<b>5</b>	<b>159</b>	<b>53</b>	<b>0.0706</b>	<b>0.0115</b>	<b>5.3184</b>	<b>0.7778</b>	<b>1</b>
17	8	135	70	7	230	57	0.0828	0.0192	5.1382	0.4939	15
18	10	200	70	10	192	75	0.1081	0.0193	4.2752	0.4939	15
19	8	135	50	8	71	58	0.0181	0.0056	5.7194	0.6528	2
20	8	135	70	6	155	62	0.0720	0.0130	4.9888	0.4939	15

where  $X_p$  is a partner solution. The new individual with improvements after learning will be accepted; otherwise rejected. In this work, a Python program was developed to compute the TLBO system for various values of the input parameters. The code of the program is given below, and the results are shown in Tables 10, 11, 12, and 13.

#### 4 Confirmation test

The optimized parameter settings for maximum  $MRR$ , minimum  $EWR$ , and  $R_a$  from analytical, RSM, GRA, and TLBO with experimental validations are done for the final optimal factors to assess the accuracy level and the results are shown in Table 14. The obtained error averages of RSM and GRA-TLBO are  $\pm 8.886\%$  and  $\pm 1.38433\%$ , respectively, which are acceptable among the other methods. This implies that a novel hybrid technique, i.e., TLBO, is more reliable to predict the desired responses than other techniques. The reason TLBO is identified as delivering the best-desired results in comparison to other methods is due to its unique capabilities for handling multi-objective optimization and the larger solution space within given constraints. TLBO offers several advantages over other methods, such as uniform

results, better handling of noisy data, and greater robustness to changes in problem parameters. Analytical methods are very simple representations, but linear relationships are not observed in practice for surface roughness. Because molten material is deposited back on the crater for a very short period of time, the integral effect of many thousands of discharges per second affects the surface finish. However, analytical models can capture the complexity of EDM in a very efficient manner. In practice,  $MRR$  does increase with an increase in peak current, pulse on-time, and gap voltage and decreases with an increase in pulse off-time.

#### 4.1 Scanning electron microscopy analysis

The field emission scanning electron microscopy (FESEM) image of the surface finishing is processed by setting the optimal values obtained from the analytical model and TLBO techniques, as delineated in Figs. 13 and 14, respectively. In Fig. 13, the controlled current value obtained from GRA-TLBO algorithm resulted in better surface finish than that of the value obtained from analytical optimization. The result shows that the formation of craters, porosity, and other surface defects depend on input parameters. Also, the presence of VC resulted in the generation of a recast layer in which the vanadium and carbon elements remained as

**Table 11** Combined population

Run no.	Combined input parameter			New response			Grade analysis grade	
	$I_p$	$t_{on}$	$V_g$	$MRR$	$EWR$	$R_a$	GRG	Rank
1	10	70	70	0.0295	0.00474	5.15718	0.535733	24
2	8	135	60	0.04875	0.00603	4.57566	0.568331	17
3	8	135	75	0.054	0.00631	4.4276	0.582127	12
4	6	70	50	0.01007	0.00128	6.82762	0.555556	19
5	8	70	60	0.01063	0.00399	5.91705	0.505189	28
6	10	200	50	0.098	0.00862	3.73189	0.706179	2
7	8	250	60	0.06938	0.009501	5.3777	0.494795	31
8	10	70	50	0.02025	0.00477	4.92045	0.543096	21
9	8	150	60	0.06513	0.00707	4.04873	0.625675	6
10	6	200	50	0.04983	0.006304	4.85258	0.54408	20
11	11	135	60	0.10852	0.00891	3.91064	0.695002	3
12	5	135	60	0.05557	0.00531	5.24866	0.542198	22
13	6	70	70	0.0191	0.002	6.63757	0.541016	23
14	6	200	70	0.06216	0.00896	5.892738	0.470673	39
15	8	140	60	0.05935	0.00708	4.117629	0.610284	8
16	8	135	45	0.05019	0.00445	4.70524	0.587577	10
17	8	135	70	0.05869	0.00632	4.54267	0.576243	14
18	10	200	70	0.08581	0.00974	4.06848	0.619579	7
19	8	135	50	0.05327	0.00505	4.4225	0.602986	9
20	8	135	70	0.05101	0.00666	4.31501	0.585318	11
21	9.48	70.00	59.86	0.02911	0.00704	5.25405	0.492765	32
22	6.79	119.73	49.84	0.04567	0.007864	5.03057	0.507559	27
23	5.09	134.98	49.78	0.05742	0.008532	5.51155	0.485745	36
<b>24</b>	<b>10.8</b>	<b>200</b>	<b>51</b>	<b>0.138438</b>	<b>0.01777</b>	<b>3.654642</b>	<b>0.784569</b>	<b>1</b>
25	8	158	53	0.07511	0.012452	4.14565	0.571288	16
26	7	125	63	0.05833	0.010425	4.84447	0.504317	29
27	10	224	48	0.12390	0.017994	4.11942	0.64646	5
28	7	208	66	0.08361	0.018986	5.02507	0.471153	38
29	8	143	73	0.06926	0.013252	4.53629	0.517964	26
30	7	172	54	0.07412	0.013346	4.45944	0.530274	25
31	6	178	57	0.07560	0.014274	4.89228	0.492305	33
32	9	156	70	0.08516	0.014968	4.09342	0.575715	15
33	8	173	59	0.08347	0.014846	4.17485	0.563744	18
34	10	193	58	0.11859	0.017781	3.77157	0.682917	4
35	8	77	45	0.01095	0.004456	5.84429	0.498231	30
36	5	159	53	0.07063	0.011489	5.31841	0.481195	37
37	7	230	57	0.08276	0.019242	5.13820	0.462219	40
38	10	192	75	0.10810	0.01933	4.27518	0.577062	13
39	8	71	58	0.01814	0.005599	5.71941	0.486248	35
40	6	155	62	0.07202	0.012967	4.98878	0.490125	34

residuals because of its poor conductivity. This phenomenon may be due to the breakdown of dielectric medium at high temperature. The high temperature during machining is the major reason for the formation of debris and surface contaminants. In EDM, elevated temperatures are unavoidable, and controlled current applied for proper pulse duration can reduce defects due to the elevated temperatures.

## 4.2 Effect of input parameters

Representative input process parameter analysis results are shown in Figs. 15, 16, and 17. The performance of EDM is sufficiently predicted by the input process parameters. The regression equations developed through

**Table 12** Candidate solution based on the non-dominance rank

Run no.	Combined input parameter			New response			Grade analysis grade	
	$I_p$	$t_{on}$	$V_g$	$MRR$	$EWR$	$R_a$	GRG	Rank
1	10.8	200	51	0.138438	0.01777	3.654642	0.784569	1
2	10	200	50	0.098	0.00862	3.73189	0.706179	2
3	11	135	60	0.10852	0.00891	3.91064	0.695002	3
4	10	193	58	0.11859	0.017781	3.77157	0.682917	4
5	10	224	48	0.12390	0.017994	4.11942	0.64646	5
6	8	150	60	0.06513	0.00707	4.04873	0.625675	6
7	10	200	70	0.08581	0.00974	4.06848	0.619579	7
8	8	140	60	0.05935	0.00708	4.117629	0.610284	8
9	8	135	50	0.05327	0.00505	4.4225	0.602986	9
10	8	135	45	0.05019	0.00445	4.70524	0.587577	10
<b>11</b>	<b>8</b>	<b>135</b>	<b>70</b>	<b>0.05101</b>	<b>0.00666</b>	<b>4.31501</b>	<b>0.585318</b>	<b>11</b>
12	8	135	75	0.054	0.00631	4.4276	0.582127	12
13	10	192	75	0.10810	0.01933	4.27518	0.577062	13
14	8	135	70	0.05869	0.00632	4.54267	0.576243	14
15	9	156	70	0.08516	0.014968	4.09342	0.575715	15
16	8	158	53	0.07511	0.012452	4.14565	0.571288	16
17	8	135	60	0.04875	0.00603	4.57566	0.568331	17
18	8	173	59	0.08347	0.014846	4.17485	0.563744	18
19	6	70	50	0.01007	0.00128	6.82762	0.555556	19
20	6	200	50	0.04983	0.006304	4.85258	0.54408	20

**Table 13** Learner phase—new process variables and objective values after interaction

Run no.	New input parameter			Bounded input parameter			New response			Grade analysis grade		
	$I_p$	$t_{on}$	$V_g$	$I_p$	$t_{on}$	$V_g$	$MRR$	$EWR$	$R_a$	GRG	Rank	Interaction
1	10.8	200	51	8.29	200.00	50.09	0.0899	0.0154	4.1715	0.5906	6	1 and 20
2	10	200	50	6.24	122.86	50.00	0.0475	0.0079	5.1921	0.5069	20	2 and 19
3	11	135	60	9.89	153.71	59.47	0.0998	0.0146	3.6774	0.7096	2	3 and 18
4	10	193	58	8.19	166.57	57.47	0.0825	0.0141	4.0901	0.5908	5	4 and 17
5	10	224	48	9.51	190.64	53.99	0.1081	0.0164	3.8107	0.7057	3	5 and 16
6	8	150	60	8.00	145.45	60.00	0.0724	0.0125	4.2443	0.5631	10	6 and 15
<b>7</b>	<b>10</b>	<b>200</b>	<b>45</b>	<b>10.00</b>	<b>193.17</b>	<b>48.21</b>	<b>0.1164</b>	<b>0.0158</b>	<b>3.7238</b>	<b>0.7716</b>	<b>1</b>	<b>7 and 14</b>
8	8	140	60	8.00	136.17	67.12	0.0680	0.0123	4.4194	0.5380	14	8 and 13
9	8	135	50	8.00	135.00	73.73	0.0649	0.0124	4.6044	0.5149	17	9 and 12
10	8	135	45	8.00	135.00	52.87	0.0634	0.0105	4.3335	0.5577	11	10 and 11
11	8	135	70	8.00	135.00	72.06	0.0658	0.0124	4.5524	0.5210	16	11 and 10
12	8	135	75	8.00	135.00	70.75	0.0664	0.0124	4.5151	0.5256	15	12 and 9
13	8	135	70	9.03	167.50	72.26	0.0887	0.0162	4.1859	0.5806	8	13 and 8
14	10	192	75	8.32	152.92	68.71	0.0778	0.0142	4.2691	0.5574	12	14 and 7
15	8	135	60	8.42	135.85	60.15	0.0708	0.0119	4.1908	0.5718	9	15 and 6
16	9	156	70	8.96	156.99	65.19	0.0872	0.0147	3.9829	0.6136	4	16 and 5
17	8	158	53	8.00	171.31	55.34	0.0816	0.0140	4.1322	0.5838	7	17 and 4
18	8	173	59	6.49	102.93	50.06	0.0347	0.0063	5.5109	0.5091	18	18 and 3
19	6	70	50	6.00	70.60	50.00	0.0105	0.0032	6.6975	0.5556	13	19 and 2
20	6	200	50	6.28	181.17	54.45	0.0746	0.0140	4.7536	0.5073	19	20 and 1

stochastic methods and the analytical models for *MRR* are compared in Fig. 15.

The results show a linear relationship between material removal rate and peak current, while pulse on-times of 135  $\mu\text{s}$ , 200  $\mu\text{s}$ , and 250  $\mu\text{s}$  and gap voltages of 50 V, 65 V, and 75 V are considered. This is mainly because of rise in energy concentration of the sparks produced between the workpiece and electrode, which in current increases thermal energy. As a result, more melting and vaporization occurs at the higher levels of current relative to low levels of current. In addition, similar increasing trend for *MRR* has been obtained by increasing the sparking time. This phenomenon is mainly related to the situation of high perforation duration of heat energy into the workpiece. Likewise, effect of input process parameter for electrode wear rate is analyzed in Fig. 16, while pulse on-times of 135  $\mu\text{s}$ , 200  $\mu\text{s}$ , and 250  $\mu\text{s}$  and peak current of 6 A, 9 A, and 11 A are considered.

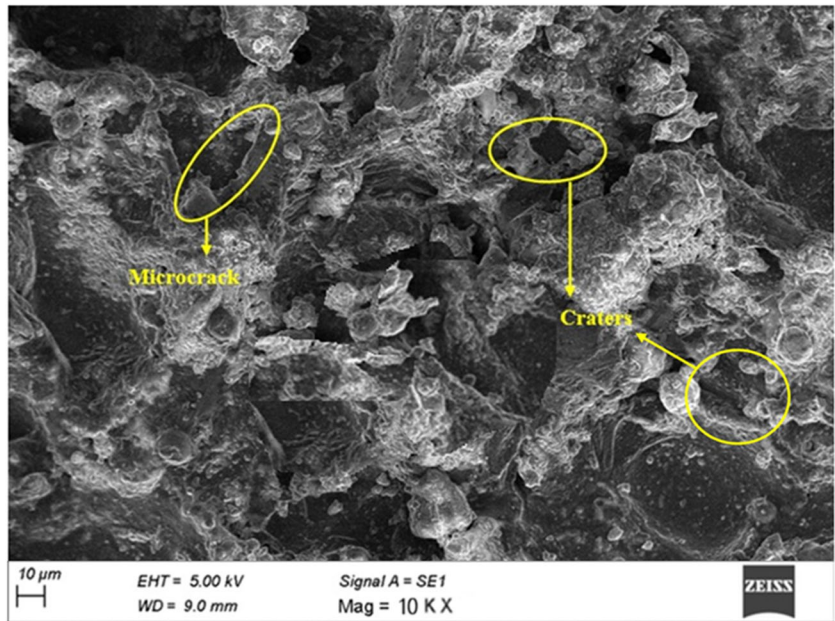
It is noted that material loss in the electrode is in direct proportional relationship with pulse duration and current. This is because of the effect of flow of charged particles between the electrodes with rise in current, which in turn causes high tool wear at high-current condition. Also, there is a loss in weight of the electrode due to an increase in voltage gap, and due to an increase in operation duration, the electrode material gets softened, which leads to material loss. In fact, electrode wear is affected by different mechanisms; knowing the evolution of electrode wear gives a better estimation of its service life. As a result, more melting and vaporization occurs at the higher levels of current relative to low levels of current. In addition, similar increasing trend for *MRR* has been obtained by increasing the sparking time. This phenomenon is mainly related to the situation of high perforation duration of heat energy into the workpiece. Likewise, effect of input process parameter for electrode wear rate is analyzed in Fig. 16, while pulse on-times of 135  $\mu\text{s}$ , 200  $\mu\text{s}$ , and 250  $\mu\text{s}$  and peak current of 6 A, 9 A, and 11 A are considered. It is noted that material loss in the electrode is in direct proportional relationship with pulse duration and current. This is because of the effect of flow of charged particles between the electrodes with rise in current, which in turn cause high tool wear at high-current condition. Also, loss in weight of the electrode due to increase in pulse duration are due to increase in operation duration; as a result, electrode material gets softened and leads to material loss.

It is proven that the electrode wear depends on the energy of the electrical discharges (input parameters) and the density of the electrode. Deterministic model validation has been done by comparing the predicted surface roughness with the stochastic results. Figure 17 shows the comparison between analytical surface roughness and stochastic values. The results show that the analytical model has no

**Table 14** Optimal parameters of analytical, RSM, GRG, VIKOR, and TLBO learner techniques and confirmatory test for optimized process parameters

Serial no.	Methods	Process parameters			Material removal rate, <i>MRR</i> (g/min)			Electrode wear rate, <i>EWR</i> (g/min)			Surface roughness, <i>R<sub>a</sub></i> ( $\mu\text{m}$ )			Compare	
		Predictor index	Parameter setting level	Parameter setting	Predicted results	Experimental results	Error %	Predicted results	Experimental results	Error %	Predicted results	Experimental results	Error %	Average error %	
1	Analytical			$I_p = 10 \text{ A}, t_{on} = 135 \mu\text{s}, V_g = 50 \text{ V}$	0.1022	0.0846	1.76	0.00638	0.00722	-0.08	4.2	4.867	66.7	21.675	
2	RSM (optimizer)			$I_p = 10 \text{ A}, t_{on} = 165 \mu\text{s}, V_g = 45 \text{ V}$	0.082	0.08958	-0.76	0.0066	0.00862	-0.2	3.742	3.999	-25.7	-8.8867	
3	GRG (optimizer)			$I_p = 11 \text{ A}, t_{on} = 175 \mu\text{s}, V_g = 45 \text{ V}$	0.0996	0.1045	-0.49	0.0076	0.00993	-0.23	3.5952	3.8871	-29.2	-9.971	
4	VIKOR (optimizer)			$I_p = 9 \text{ A}, t_{on} = 168 \mu\text{s}, V_g = 45 \text{ V}$	0.0769	0.0699	0.7	0.0064	0.00871	-0.23	3.8136	4.1002	-28.7	-9.397	
5	TLBO learner			$I_p = 10 \text{ A}, t_{on} = 193 \mu\text{s}, V_g = 48 \text{ V}$	0.1164	0.10995	0.645	0.0158	0.01192	0.39	3.7238	3.6926	3.12	1.38433	

**Fig. 13** FESEM micrograph of surface finishing using optimized factors from analytical model



linear relationship with practical observation. The surface roughness of the resulting craters usually represents the peak-to-valley roughness. The maximum depth crater of the damaged or machined layer is taken as 2.5–4 times the average surface roughness  $R_a$ . It is well known that the melted material is not fully flushed from the crater; a considered amount of melted material again solidifies in the crater in the form of a recast layer. As a result, wider and deep craters are produced on the harsh surface finishing. Indeed, this phenomenon can be reduced through good flushing pressure to particles and reduced intensity of thermal energy with increase in pulse interval.

The machinability of the developed LM25Al/VC composite was evaluated using spark EDM by varying the process variables. The machining metrics (i.e., material removal rate, electrode erosion rate, and surface roughness) were measured and optimized using different optimization methods like RSM, GRG, VIKOR, and TLB. In the same way, phenomenological three-dimensional representations of these optimizer methods are shown in Fig. 18. The three-dimensional result shows that TLBO learner methods give consistent GRG output among other optimizer indexes. Figure 18 shows a decreasing trend in TLBO learners'

**Fig. 14** FESEM micrograph of surface finishing using optimized factors from TLBO

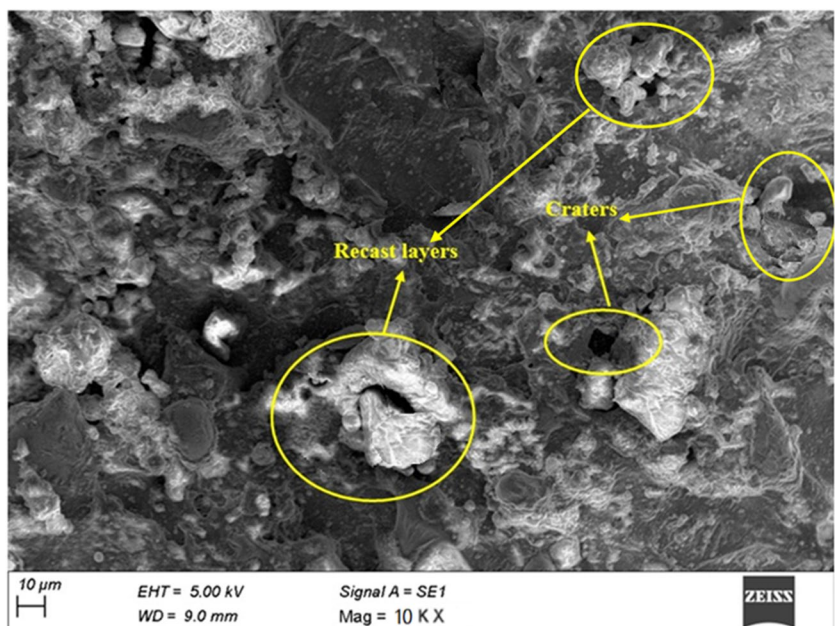


**Fig. 15** Material removal rate versus peak current with different pulse on-time and gap voltage

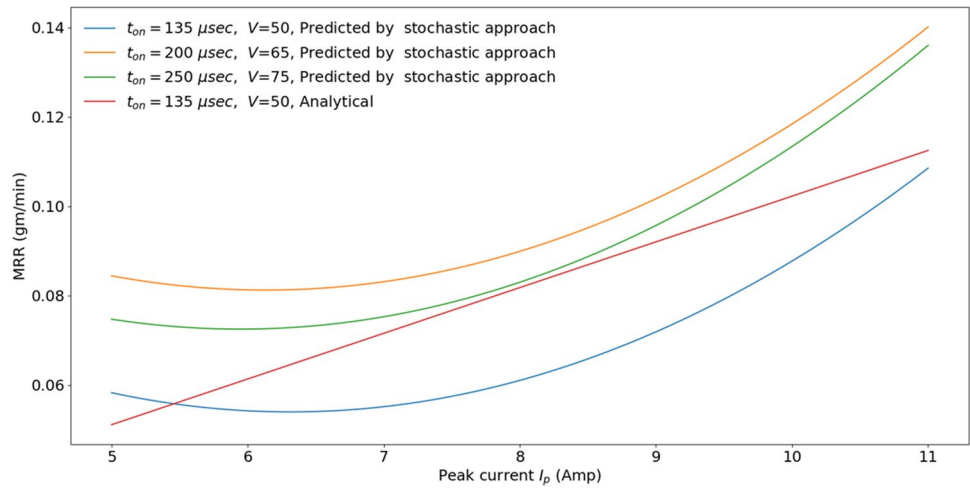


**Fig. 16** Electrode wear rate versus gap voltage with different pulse on-time and peak current

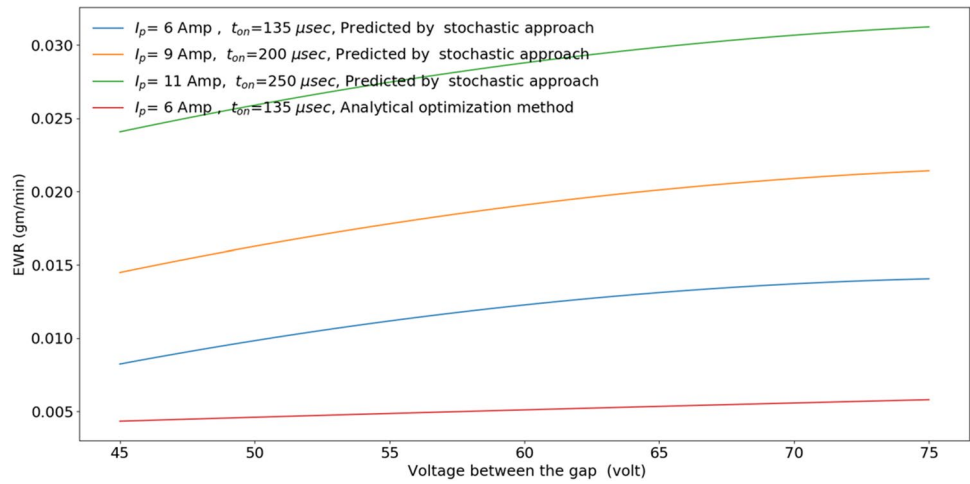


**Fig. 17** Surface roughness versus pulse on-time with different peak current and gap voltage

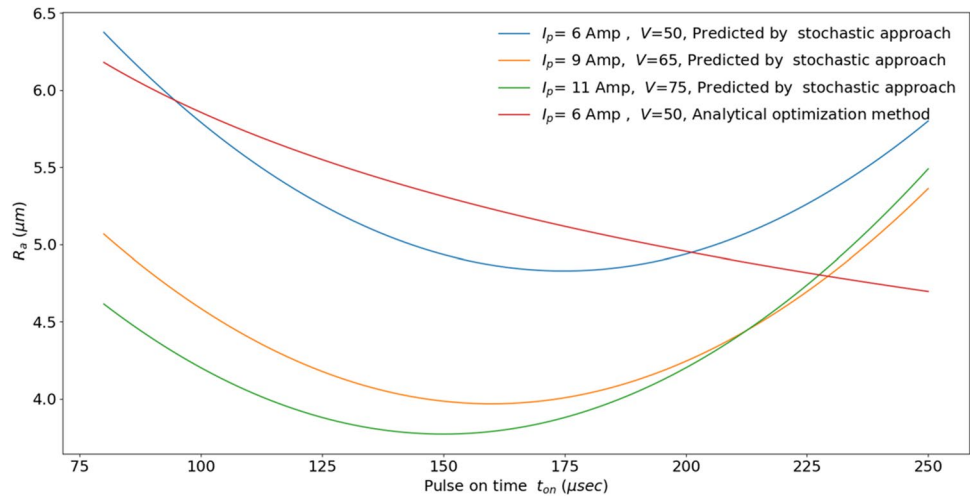
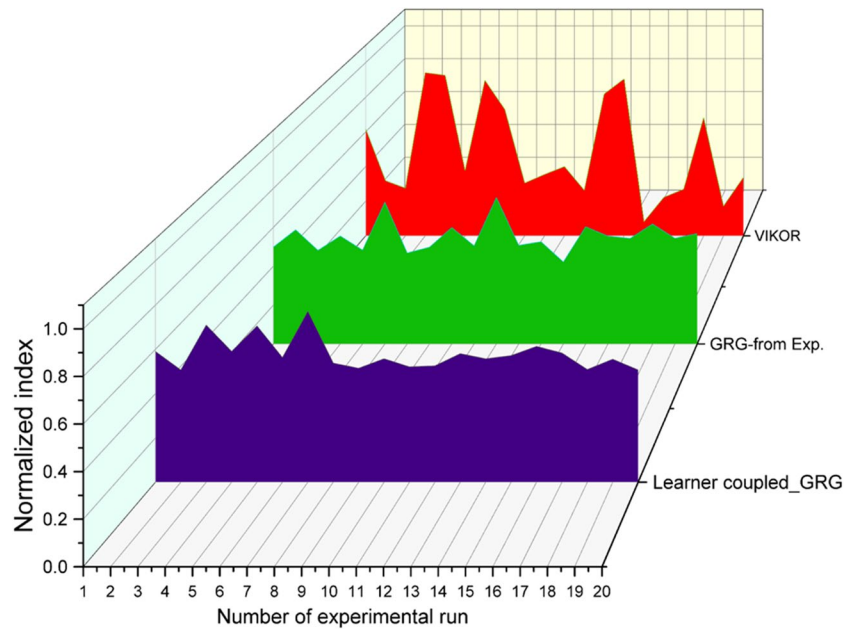


**Fig. 18** The 3D profile of optimizer methods (TLBO learner GRG, RSM-coupled GRG, and VIKOR) versus number of experimental run



output responses with iteration in interaction and process parameters. This is mainly due to the increased consistency of output responses.

## 5 Conclusion

In this work, analytical model and four decision-making multi response optimization techniques (RSM-coupled GRG, VIKOR, and TLBO) have been adopted to optimize the process parameters using performance characteristics, viz., *EWR*, *MRR*, and  $R_a$ , during EDM operation of LM25AL/VC composite with copper electrode. Based on the above investigation, the following conclusions have been drawn:

1. Analytical models are very simple, less cost-effective, and time-effective, among other techniques, but linear relationships are not observed in practice for surface roughness. Because the melted material solidifies again on the crater and forms the recast layers, however, these simplified models can capture the complexity of EDM in a very efficient manner with effective engineering judgments. Especially, the analytical approximation of the *MRR* and *TWR* is a promising method for approximating process performance analysis.
2. The validation tests were carried out to find the effectiveness of the developed models. In that, TLBO learner phase-coupled GRG offered good predicting ability of the responses with lesser error average of  $\pm 1.384\%$  among other predictor (error average).
3. Confidence level (*R*-sq) of 96.59% and 99.6% for *MRR* and *EWR*, respectively; ANOVA results show that pulse on-time and peak current are the most significant parameters for the responses using the RSM method.
4. EDS graph of unmachined LM25AL/VC showed that the constituents of base metal and reinforcement are uniform distributed in matrix material.
5. The pulse current was the most dominating parameter that effects on *MRR* and *EWR* and then followed by pulse duration
6. In terms of dimensional deviation, a lower  $I_p$  and  $t_{on}$  with a higher gap voltage can be compensating. However, the less material removed and the finer surface finishing.
7. In terms of *EWR*, the lower the pulse on-time and high peak current, the better the solution. It has been discovered that high temperatures cause the electrode to erode and melting more quickly; resulting *EWR* is fast. Because of the strong current, high temperatures occur, causing additional erosion of the electrode surface.
8. The present study has been attempted considering  $I_p$ ,  $t_{on}$ , and  $V_g$  as input parameters. However, more number of process inputs can be included in the future research based on the availability and functionality of the EDM setup. The present work was limited to the EDM of LM25Al/VC composite considering advance composite material in manufacturing industries.

## Appendix A

Optimization parameters that obtained from curve-fitting through python programming

$G=0.00025$ ,  $M=36.991$ ,  $a1=-0.5018$ ,  $b1=-0.2417$ ,  $c1=0.04579$ ,  $N=0.00357$ ,  $a2=0.6384$ ,  $b2=0.7848$ ,  $c2=0.5708$

\* Python program to solve problems, for example. In fact, the method is the same for EWR.

```
import numpy as np
from scipy.optimize import curve_fit
import pandas as pd
#Surface Roughness
df = pd.read_excel("experimentaldataRa.xlsx")
# Extract the data into separate arrays
Ip = x1 = df['x1'].values
ton = x2 = df['x2'].values
Vg = x3 = df['x3'].values
Ra = y = df['y'].values
# Define the model function
def model(x, M, a1, b1, c1):
return (M * (x1 ** a1) * (x2 ** b1) * (x3 ** c1))
#Fit the model into data
popt, _ = curve_fit(model, (x1, x2, x3), y, p0=(1, 1, 1, 1))
#Extract the optimized parameters
M_opt, a1_opt, b1_opt, c1_opt = popt
#Print the optimized parameters
print(f"M_opt: {M_opt}")
print(f"a1_opt: {a1_opt}")
print(f"b1_opt: {b1_opt}")
print(f"c1_opt: {c1_opt}")
```

**Acknowledgements** The authors highly acknowledge the NORHED II NORAD organization. The authors also gratefully acknowledged the facilities provided by Stavanger and Jimma Universities.

**Author contribution** M. A. T. did the former analysis and wrote the paper; H. G. L. was the supervisor and did the critical review of the manuscript.

**Funding** Open access funding provided by University of Stavanger & Stavanger University Hospital. This research was supported by the NORHED II project INDMET grant (grant nr. 62862).

## Declarations

**Conflict of interest** The authors declare no competing interests.

**Open Access** This article is licensed under a Creative Commons Attribution 4.0 International License, which permits use, sharing, adaptation, distribution and reproduction in any medium or format, as long as you give appropriate credit to the original author(s) and the source, provide a link to the Creative Commons licence, and indicate if changes were made. The images or other third party material in this article are included in the article's Creative Commons licence, unless indicated otherwise in a credit line to the material. If material is not included in the article's Creative Commons licence and your intended use is not permitted by statutory regulation or exceeds the permitted use, you will

need to obtain permission directly from the copyright holder. To view a copy of this licence, visit <http://creativecommons.org/licenses/by/4.0/>.

## References

- Kumar A, Sharma R (2020) Multi-response optimization of magnetic field assisted EDM through desirability function using response surface methodology. *J Mech Behav Mater* 29:19–35. <https://doi.org/10.1515/jmbm-2020-0003>
- Gupta K, Gupta K (2019) Developments in nonconventional machining for sustainable production: a state-of-the-art review. *Proceedings of the Inst of Mech Engi, Part C: J Mech Eng Sci* 233:4213–4232
- Sivaraman B, Padmavathy S, Jothiprakash P, Keerthivasan T (2021) Multi-response optimisation of cutting parameters of wire EDM in titanium using response surface methodology. *Appl Mech Mater* 854:93–100. <https://doi.org/10.4028/www.scientific.net/amm.854.93>
- Aleksendric D, Carlone P (2015) Introduction to composite materials. *Sci Direct* 5:1–5
- Abbas N, Solomon G, Fuad M (2009) A review on current research trends in electrical discharge machining (EDM). *Int J Mach Tools and Manuf* 47:1214–1228
- Sun Z, Ahuja R (2010) Mechanical properties of vanadium carbide and a ternary vanadium tungsten carbide. *Sol Sta Comm* 150:697–700
- Bodunrin M, Alaneme K, Chown L (2015) Aluminium matrix hybrid composites: a review of reinforcement philosophies; mechanical, corrosion and tribological characteristics. *J Mat Res and Tech* 4:434–445
- Yoo K, Kwon T, Kang S (2014) Development of a new electrode for micro-electrical discharge machining (EDM) using Ti(C,N)-based cermet. *Int J of Prec Engi and Manuf* 15:609–616
- Selvarajan L, Narayanan S, Jeyapaul R (2015) Optimization of EDM hole drilling parameters in machining of MoSi<sub>2</sub>-SiC intermetallic/composites for improving geometrical tolerances. *J Adv Manuf Syst* 14:259–272. <https://doi.org/10.1142/S0219686715500171>
- Kumar D, Mer S, Payal S, Kumar K (2021) Residual stress modeling and analysis in Aisi A2 steel processed by an electrical discharge machine. *Mater Tehnol* 56:65–72. <https://doi.org/10.17222/mit.2021.325>
- Ashebir D, Mengeshat A, Sinha K. An insight into mechanical and metallurgical behavior of hybrid reinforced aluminum metal matrix composite. *J Adv in Mater Sci and Engi* 2022; <https://doi.org/10.1155/2022/7843981>
- Pradhan K, Biswas K. Modeling of residual stresses of edmed Aisi 4140 steel, *Proceedings of the International Conference on Recent Advances in Materials, Proc and Chara* 2008; 49-55. A.P. India
- Kruth L, Stevens L, Froyen L (1995) Study of the white layer of a surface machined by die-sinking electrical-discharge machining. *CIRP Annals* 44:169–172. [https://doi.org/10.1016/S0007-8506\(07\)62299-9](https://doi.org/10.1016/S0007-8506(07)62299-9)
- Rajmohan T, Vinayagamoorthy R, Mohan K (2019) Review on effect machining parameters on performance of natural fibre-reinforced composites (NFRCS). *J Therm Compos Mater* 32:1282–1302
- Yadav V, Jain V, Dixit P (2002) Thermal stresses due to electrical discharge machining. *Int J Mach Tools and Manuf* 42:877–888. [https://doi.org/10.1016/S0890-6955\(02\)00029-9](https://doi.org/10.1016/S0890-6955(02)00029-9)
- Luzia O, Laurindo H, Soares C, Torres D, Mendes L, Amorim. (2019) Recast layer mechanical properties of tool steel after electrical discharge machining with silicon powder in the



- dielectric. *Int J Adv Manuf Technol*:10315–10328. <https://doi.org/10.1007/s00170-019-03549-w>
17. Sundriyal S, Vipin S (2020) Study on the influence of metallic powder in near-dry electric discharge machining. *Stroj Vestnik/J Mech Eng* 66:243–253. <https://doi.org/10.5545/sv-jme.2019.6475>
  18. Sathish T (2019) Experimental investigation of machined hole and optimization of machining parameters using electrochemical machining. *J Mater Res and Technol* 8:4354–4363
  19. Daneshmand S, Masoudi B, Monfared V (2017) Electrical discharge machining of Al/7.5% Al<sub>2</sub>O<sub>3</sub> MMCs using rotary tool and Al<sub>2</sub>O<sub>3</sub> powder. *Surf Rev Lett* 24:1–17. <https://doi.org/10.1142/S0218625X17500184>
  20. Nagarajan P, Murugesan K, Natarajan E (2019) Optimum control parameters during machining of LM13 aluminum alloy under dry electrical discharge machining (EDM) with a modified tool design. *Medziagotyra* 25:270–275. <https://doi.org/10.5755/joi.ms.25.3.20899>
  21. Klocke FH, T, Zeis M, Klink A. (2018) Experimental investigations of cutting rates and surface integrity in wire electrochemical machining with rotating electrode. *Procedia CIRP* 68:725–730
  22. Gudur P (2018) Effect of silicon carbide powder mixed EDM on machining characteristics of SS 316L material. *Int J Innov Res Sci Eng Technol* 08:8133–8141. <https://doi.org/10.15680/ijirset.2015.0404027>
  23. Ablyaz TR, Shlykov ES, Muratov KR, Sidhu SS (2021) Analysis of wire-cut electro discharge machining of polymer composite materials. *Micromachines* 12(5):571
  24. Chow M, Yang D, Lin T, Chen F (2008) The use of SiC powder in water as dielectric for micro-slit EDM machining. *J Mater Process Technol* 195(1–3):160–170. <https://doi.org/10.1016/j.jmatprotec.2007.04.130>
  25. Fadhil S, Aghdeab S (2020) Effect of powder-mixed dielectric on EDM process performance. *J Eng Technol* 38:1226–1235. <https://doi.org/10.30684/etj.v38i8a.554>
  26. Daneshmand S, Kahrizi E, Abedi E (2013) Influence of machining parameters on electro discharge machining of NiTi shape memory alloys. *Int J Electroch Sci* 8:3095–3104
  27. Dwivedi P, Choudhury K (2016) Effect of tool rotation on MRR, TWR, and surface integrity of AISI-D3 steel using the rotary EDM process. *Mater Manuf Process* 31:1844–1852
  28. Acharya G, Jain K, Batra L (1986) Multi-objective optimization of the ECM process, vol 8. Butterworth Co (Publishers) Ltd, pp 288–296
  29. Kurnia W, Tan P, Yeo S, Wong M (2008) Analytical approximation of the erosion rate and electrode wear in micro electrical discharge machining. *J Micromech Microeng* 8:1–8
  30. Shrivastava K, Dubey K (2014) Electrical discharge machining-based hybrid machining processes: a review. *Proc IMechE, Part B: J Eng Manuf* 228:799–825
  31. Biswas S, Singh Y, Mukherjee M (2022) Design of multi-material model for wire electro-discharge machining of SS304 and SS316 using machine learning and MCDM techniques. *Arab J Sci Eng* 47:15755–15778. <https://doi.org/10.1007/s13369-022-06757-x>
  32. Naik M, Narendranath S (2017) Influence of process parameters on material removal rate in wire electric discharge turning process of INCONEL 718. *Int J Adv Res Sci Eng* 25:224–232
  33. Ming Z, Fuzhu H, Isago S (2008) A time-varied predictive model for EDM process. *Int J of Mach Tool and Manuf* 48(15):1668–1677
  34. Kiran P, Mohanty S, Das K (2021) Surface modification through sustainable micro-EDM process using powder mixed bio-dielectrics. *Mater Manuf Process* 1:1–12. <https://doi.org/10.1080/10426914>
  35. Valaki J, Rathod P, Khatri B (2015) Environmental impact, personnel health and operational safety aspects of electric discharge machining: a review. *Proc. IME B: J Eng Manufact* 229:1481–1491
  36. Hassan H, Arman B, Behnoosh M (2014) Performance analysis of manufacturing systems using deterministic and stochastic Petri Nets. *J Math Comp Sci* 11:1–12
  37. Manjaiah S, Narendranath A, Basavarajappa S (2018) Investigation on material removal rate, surface and subsurface characteristics in wire electro discharge machining of Ti<sub>50</sub>Ni<sub>50-x</sub>Cu<sub>x</sub> shape memory alloy processing. *IME: J Mater Des Appl* 232:164–177
  38. Cooke F, Crookall J (1973) An investigation of some statistical aspects of electro-discharge machining. *Intern J Mach Tool Des Res* 13:271–286
  39. Singh R, Singh P, Rajeev T (2022) Machine learning algorithms based advanced optimization of EDM parameters: an experimental investigation into shape memory alloys. *Sens Intern* 3:1–13
  40. Shao M, Han Z, Sun J, Xiao C, Zhang S, Zhao Y (2020) A review of multi-criteria decision making applications for renewable energy site selection. *Renew Energ* 157:377–403
  41. Rao R, Kalyankar V (2011) Parameters optimization of advanced machining processes using TLBO algorithm. EPPM, Singapore, pp 20–21
  42. Manish G, Pradhan K (2018) Optimization the machining parameters by using VIKOR method during EDM process of titanium alloy. *Mater Today: Proc* 5:7486–7495
  43. Singaravel B, Prasad D, Shekar C, Rao M, Reddy G (2020) Optimization of process parameters using hybrid Taguchi and VIKOR method in electrical discharge machining process. In: *In Advanced Engineering Optimization Through Intelligent Techniques*. Springer, Singapore, pp 527–536
  44. Pratap R, Sharma V, Kumar R Optimization of response parameter of machining En31 while electro-dischargemachiningusing TLBO. *Mater Today: Proc*. <https://doi.org/10.1016/j.matpr.2023.02.121>
  45. Karthikeyan G, Jinu G, Thankachi R (2019) mechanical properties and metallurgical characterization of LM25/ZrO<sub>2</sub> composites fabricated by stir casting method. *Revista Matéria* 24:1–13
  46. Kamal U, Abhijit S, Himadri M (2023) Machinability assessment of wire-EDM using brass wire for C-45 steel applying VIKOR-AHP. *Surfa Rev Lett*:1–18. <https://doi.org/10.1142/S0218625X23500890>
  47. Mausam K, Tiwari M, Sharma K, Singh R (2013) Process parameter optimization for maximum material removal rate in high-speed electro-discharge machining. *International Symposium on Engineering and Technology*, 9–10 January 2014 organized by KJEL's Trinity College of Engineering and Research, Pune. *Int J Curr Eng Technol* 239–244
  48. Srikanth R, Singaravel B, Vinod P, Aravind P, Subodh D (2021) Optimization of process parameters in electric discharge machining process of Ti-6Al-4V alloy using hybrid Taguchi based MOORA method. *IOP Conf. Series: J Mater Sci and Eng* 1057:12–64. <https://doi.org/10.1088/1757-899X/1057/1/012064>
  49. Paulo A, Vishad V, Ana A, Sergio S, Boris JB (2021) Stochastic approach for product costing in manufacturing processes. *Mathematics* 9:2238. <https://doi.org/10.3390/math9182238>
  50. Hosni J, Lajis A (2019) Experimental investigation and economic analysis of surfactant (pan-20) in powder mixed electrical discharge machining (PMEDM) of AISI D2 hardened steel. *Mach Sci Technol* 24:398–424. <https://doi.org/10.1080/10910344.2019.1698609>
  51. Ehsan G, Pakseres H, Masoud A, Kamyar S, Ebadzadeh T (2016) Vanadium carbide reinforced aluminum matrix composite prepared by conventional, microwave and spark plasma sintering. *J Alloy Comp* 688:527–533. <https://doi.org/10.1016/j.jallcom.2016.07.063>
  52. Rao P, Das K, Murty K, Chakraborty M (2006) Microstructural and wear behavior of hypoeutectic Al-Si alloy (LM25)

- grain refined and modified with Al-Ti-C-Sr master alloy. *Wear* 26:133–139
53. Gangil M, Pradhan M (2018) Optimization of the machining parameters by using VIKOR method during EDM process of titanium alloy. *Mater Today Proc* 5:7486–7495
  54. Balanou M, Karmiris-Obratański P, Leszczyńska-Madej B, Papazoglou L, Markopoulos P (2021) Investigation of surface modification of 60CrMoV18-5 steel by EDM with Cu-ZrO<sub>2</sub> powder metallurgy green compact electrode. *Machines* 11:268. <https://doi.org/10.3390/machines9110268>
  55. Singaravel B, Shekar KC, Reddy GG, Prasad SD (2020) Experimental investigation of vegetable oil as dielectric fluid in electric discharge machining of Ti-6Al-4V. *Ain Shams Eng J* 2019:143–147. <https://doi.org/10.1016/j.asej.2019.07.010>
  56. Iacob-Tudose T, Mamaliga I, Iosub VT (2021) A review of thermophysical properties and their impact on system design. *Nanomaterials* 11:3415. <https://doi.org/10.3390/nano11123415>
  57. Singaravel B, Prasad S, Shekar K, Rao K, Reddy G (2019) Optimization of process parameters using hybrid Taguchi and VIKOR method in electrical discharge machining process. *J. Adv Eng Optim Through Intelligent Techniques* 527–536
  58. Bisaria H, Shandilya P (2019) Study on crater depth during material removal in WEDC of Ni-rich nickel–titanium shape memory alloy. *J Braz Soc Mech Sci Eng* 41:157
  59. Selvarajan L, Palani K, Srinivasan P (2018) Experimental investigation on EDM of Si<sub>3</sub>N<sub>4</sub>-TiN using grey relational analysis coupled with teaching-learning-based optimization algorithm. *Int J Comput Mater Sci Surf Eng* 7:104. <https://doi.org/10.1504/ijcmsse.2018.10013789>
  60. Faisal N, Kumar K (2018) Optimization of machine process parameters in EDM for EN31 using evolutionary optimization techniques. *Technologies* 6:54. <https://doi.org/10.3390/technologies6020054>
  61. Bulent E, Oktay E, Tekkaya A, Erden A (2005) Residual stress state and hardness depth in electric discharge machining: de-ionized water as dielectric liquid. *Mach Sci Technol* 9:39–36, ISSN: 1091-0344 print/1532-2483 online. <https://doi.org/10.1081/MST-200051244>
  62. Kumar PR (2016) Experimental investigation and optimization of EDM process parameters for machining of aluminum boron carbide (Al-B4C) composite. *J Mach Sci Technol* 20(2):330–348. <https://doi.org/10.1080/10910344.2016.1168931>
  63. Mahanta S, Chandrasekaran S, M. Samanta S, Arunachalam M. (2018) EDM investigation of Al 7075 alloy reinforced with B4C and fly ash nanoparticles and parametric optimization for sustainable production. *J Braz Soci Mech Sci Eng* 40:1–17. <https://doi.org/10.1007/s40430-018-1191-8>
  64. Dwivedi P, Choudhury K (2016) Effect of tool rotation on MRR, TWR, and surface integrity of AISI-D3 steel using the rotary EDM process. *Mater Manuf Process* 31:1844–1852. <https://doi.org/10.1080/10426914.2016.1140198>
  65. Ramaswamy A, Perumal V (2016) Multi-objective optimization of drilling EDM process parameters of LM13 Al alloy–10ZrB2–5TiC hybrid composite using RSM. *J Braz Soc Mech Sci Eng* 42:1–18. <https://doi.org/10.1007/s40430-020-02518-9>
  66. Asokan P, Kumar R, Jeyapaul R, amd Santhi M. (2008) Development of multi-objective optimization models for electrochemical machining process. *Int J Adv Manuf Technol* 39:55–53
  67. Khullar R, Sharma N, Kishore S, Sharma R (2017) RSM- and NSGA-II-based multiple performance characteristics optimization of edm parameters for AISI 5160. *Arab J Sci Eng* 42:1917–1928. <https://doi.org/10.1007/s13369-016-2399-5>
  68. Srinivasan P, Palani K, Balamurugan S (2021) Experimental investigation on EDM of Si<sub>3</sub>N<sub>4</sub>TiN using grey relational analysis coupled with teaching-learning-based optimization algorithm. *Ceram Int* 47:19153–19168. <https://doi.org/10.1016/j.ceramint.2021.03.262>

**Publisher's Note** Springer Nature remains neutral with regard to jurisdictional claims in published maps and institutional affiliations.